MAXWELL
S-CUBED Division

SSS-TR-91-12241

Two and Three Dimensional Numerical Modeling of Surface Waves from Underground Explosions, Analysis of Data from the Soviet JVE, and Magnitude/Yield Relations for East Kazakh Explosions

J. L. Stevens
T. G. Barker
S. M. Day
K. L. McLaughlin
B. Shkoller

Annual Report
CDRL 002A2

Sponsored by:
DEFENSE ADVANCED RESEARCH PROJECTS AGENCY (DoD)

Monitored by:
U. S. AIR FORCE TECHNICAL APPLICATIONS CENTER
Under Contract No. F08606-89-C-0022

February 1991

P. O. Box 1620, La Jolla, California 92038-1620
(619) 453-0060

REPORT DOCUMENTATION PAGE

Form Approved
OMB No. 0704-0188

1. AGENCY USE ONLY *(Leave blank)*	2. REPORT DATE	3. REPORT TYPE AND DATES COVERED
	January 1991	Annual Report

4. TITLE AND SUBTITLE
Two and Three Dimensional Numerical Modeling of Surface Waves from Underground Explosions, Analysis of Data from the Soviet JVE, & Magnitude/Yield Relations for E. Kazakh Explosions

5. FUNDING NUMBERS
C - F08606-89-C-0022

6. AUTHOR(S)
K. L. McLaughlin, T. G. Barker, S. M. Day, B. Shkoller and J. L. Stevens

7. PERFORMING ORGANIZATION NAME(S) AND ADDRESS(ES)
S-CUBED, A Division of Maxwell Laboratories, Inc.
P.O. Box 1620
La Jolla, CA 92038-1620

8. PERFORMING ORGANIZATION REPORT NUMBER
SSS-TR-91-12241

9. SPONSORING/MONITORING AGENCY NAME(S) AND ADDRESS(ES)
Defense Advanced Research Projects Agency
3701 N. Fairfax, Suite 717
Arlington, VA 22209-1714

10. SPONSORING/MONITORING AGENCY REPORT NUMBER

11. SUPPLEMENTARY NOTES

12a. DISTRIBUTION/AVAILABILITY STATEMENT
Approved for public release; distribution is unlimited.

12b. DISTRIBUTION CODE

13. ABSTRACT *(Maximum 200 words)*

We perform three dimensional finite difference simulation of surface waves generated at the Amchitka test site and find that the Aleutian arc structure causes higher amplitudes to the east relative to the north and south, and that this structure can also generate rapid amplitude changes over a small range of azimuths and generate Love waves with substantial amplitudes. A series of two-dimensional finite difference simulations show that long period surface wave amplitudes can be sharply reduced by detonation on an island, in a mountain, or in a high velocity medium embedded in a low velocity medium, however the topography and bathymetry of the Amchitka test site are too gentle to cause a significant amplitude reduction.

Moment tensor inversions are performed on the JVE and four other Soviet explosions. The JVE is found to be a low tectonic release event with an F factor of 0.2. Data recorded by the University of Nevada, Reno, at three stations within 300 km of the JVE are inverted to determine the shear velocity structure to depths of approximately 30 km near the Shagan River test site. A maximum likelihood analysis of the yields released in the paper by Bocharov shows that m_b for a 20 KT East Kazakh explosion is 5.53.

14. SUBJECT TERMS			15. NUMBER OF PAGES
Amchitka	Rayleigh Waves	Bocharov	51
Finite Difference	JVE		16. PRICE CODE
Surface Waves	Explosion Seismology		

17. SECURITY CLASSIFICATION OF REPORT	18. SECURITY CLASSIFICATION OF THIS PAGE	19. SECURITY CLASSIFICATION OF ABSTRACT	20. LIMITATION OF ABSTRACT
Unclassified	**Unclassified**	**Unclassified**	

CLASSIFIED BY:
DECLASSIFY ON:

Abstract

This report is a summary of work in progress at S-CUBED on numerical modeling of surface waves generated by explosions in complex structures, and analysis of data from Soviet explosions using information obtained as part of the Joint Verification Experiment (JVE) and other information recently released by the Soviet Union.

A three dimensional finite difference simulation of surface waves generated at the Amchitka test site is performed to look at the effects of Aleutian Arc structure on surface wave generation and propagation. We find that the Aleutian arc structure causes higher amplitudes to the east relative to the north and south, and that this structure can also generate rapid amplitude changes over a small range of azimuths and generate Love waves with substantial amplitudes. A series of two-dimensional finite difference simulations are performed to look at the effect of island/ocean boundaries and topography on surface wave generation. We find that long period surface wave amplitudes can be sharply reduced by detonation on an island, in a mountain, or in a high velocity medium embedded in a low velocity medium, however the topography and bathymetry of the Amchitka test site are too gentle to cause a significant amplitude reduction.

Moment tensor inversions are performed on the JVE and four other Soviet explosions. The JVE is found to be a low tectonic release event with an F factor of 0.2. Data recorded by the University of Nevada, Reno, at three stations within 300 km of the JVE are inverted to determine the shear velocity structure to depths of approximately 30 km near the Shagan River test site. A maximum likelihood analysis of the yields released in the paper by Bocharov is performed to determine a magnitude yield relation for the East Kazakh test sites. Although exact yields are available for only a small subset of events, the events with yield ranges put additional constraints on the magnitude/yield relation. Because of this, the magnitude/yield relation at 20 KT is very well determined.

Table of Contents

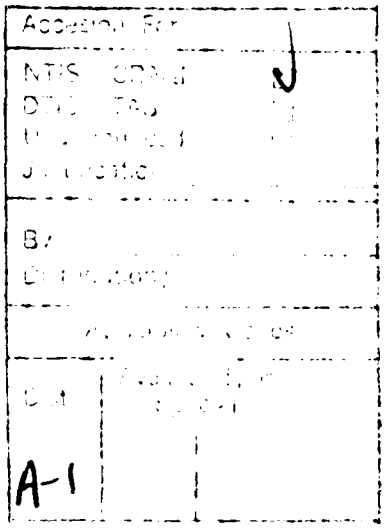

List of Illustrations

List of Illustrations (Continued)

List of Illustrations (Continued)

1. Introduction

This report is a summary of work in progress at S-CUBED on numerical modeling of surface waves generated by explosions in complex structures, and analysis of data from Soviet explosions using information obtained as part of the Joint Verification Experiment and other information recently released by the Soviet Union. The numerical modeling of surface waves is divided into two parts: three-dimensional finite difference simulations of explosions at the Amchitka test site, and two-dimensional simulations of the effects of the island/ocean interface. A detailed report on the three-dimensional calculations is being submitted separately (McLaughlin, *et al.*, 1991), and the results are summarized in this report.

The three-dimensional modeling of the Amchitka explosions is motivated by the strong azimuthal variations observed in the Rayleigh waves from these explosions. Rayleigh wave amplitudes observed at Canadian and northern United States stations were very large compared to Rayleigh wave amplitudes observed in the southern United States. A possible explanation of this is that the Aleutian Arc caused focusing of Rayleigh waves in northern Canada and defocusing in the southern United States. To model the wave propagation from these explosions, we used a model for Aleutian Arc structure based on recent work by Boyd and Creager (1991), with a grid designed to model surface waves in the 20 to 40 second period range. The results of these calculations show that the deep structure of the subduction zone (the downgoing slab), has little effect on surface waves, however the variation in crustal thickness parallel and normal to the Aleutian Arc has a pronounced effect on the surface wave amplitudes. In particular, significantly larger surface wave amplitudes are generated toward the east than toward the north and south, and Love waves with amplitudes of 1/4 to 1/3 of the peak Rayleigh wave amplitude are generated toward the northeast and southwest. Furthermore, the Aleutian structure is capable of causing rapid amplitude changes as a function of azimuth in certain directions. These rapid amplitude changes are interference effects and may be sensitive to fine details of the structure. These results can explain some of the anomalous amplitude variations observed from these explosions, however a substantial amount of tectonic release is still required to explain the observed azimuthal radiation pattern.

The series of two-dimensional calculations of an explosion on an island is motivated by the work of von Seggern (1978) and others who found a possible surface wave magnitude bias between Amchitka and NTS, and suggested that surface waves generated by an explosion on an island might differ from those generated by a mid-continent explosion. The results of the calculations show that detonation on an island, in a mountain, or near a lower velocity boundary can dramatically affect the surface wave amplitudes. The reason for this is that the horizontal stress components that generate surface waves for a shallow source are relieved by the presence of a vertical boundary in the same manner that the vertical stress components are relieved by the free surface boundary condition. The topography and bathymetry of the Amchitka test site, however, is too gentle to cause a significant amplitude reduction.

We also report on results of analysis of data from the Joint Verification Experiment and other information recently released by the Soviet Union. There are three parts to this analysis. First, we perform a moment tensor inversion of surface waves from the JVE and four other Shagan River explosions recorded at GDSN and CDSN stations. Inversion of the JVE data shows that the Soviet JVE was a low tectonic release event with an F factor of 0.2. Second, we invert 1 to 10 second surface waves recorded at three stations operated by the University of Nevada, Reno, to determine the structure of the upper 30 km of the earth near the Shagan River test site. Third, we perform a maximum likelihood analysis of the information contained in the recent paper by Bocharov, *et al.* (1989). The maximum likelihood analysis makes use of yield ranges as well as yields, and this additional information adds some very strong constraints to the magnitude/yield relation. In particular, since many yields are given as "less than 20 KT," or "between 20 and 150 KT," the yield at 20 KT is very well defined. We estimate the mean mb (20 KT) = 5.530 ± 0.016, and the standard deviation of the magnitude yield relation at 20 KT is 0.059 ± 0.012. Using the entire data set, we obtain mb = 4.520 ± 0.063 + 0.760 ± 0.040 log (Yield). These relations were derived using the UK magnitudes given in Vergino's (1989) summary of the Bocharov paper.

2. Three-Dimensional Modeling of Surface Waves from the Amchitka Explosions.

Rayleigh waves from the three Amchitka explosions LONGSHOT, MILROW, and CANNIKIN show very strong amplitude variations as a function of azimuth. Part of this variation can be explained by tectonic strain release (Toksos and Kehrer, 1972; Stevens and McLaughlin, 1989), however the change in amplitudes occurs over such a narrow azimuthal range in some cases that it is difficult to explain all of the variation by this mechanism. In Figure 2.1, we show relative amplitudes of path corrected Rayleigh waves for these three events. Notice the very strong decrease in amplitudes between approximately 50 degrees and 90 degrees (the range of azimuths between Canada and the southern United States). The purpose of this study is to see if all or part of the azimuthal variation can be explained by propagation characteristics of the Aleutian arc, and to determine the effect of this structure on explosion yield estimates.

Three-dimensional linear elastic finite difference calculations were used to investigate effects of near-source scattering on long-period surface waves radiated by shallow explosions located in the Aleutian subduction zone. Our objective was to accurately model elastic waves with periods 20 seconds or longer over a region extending 400 km from Amchitka island in all directions. To achieve this resolution and spatial extent efficiently, we generated a finite difference grid with an inner, finely gridded region with 6 km spacing. Outside this high-resolution inner grid, the spacing was slowly expanded at a constant rate of increase. The inner portion of the grid was 70x70x140 grid points (420 by 420 by 840 km). The time step was 0.25 sec. Figure 2.2 illustrates this use of an expanding, attenuating grid outside the inner grid. The total grid used in the computation was 100 by 100 by 200 or 2 million grid points. A 840 by 840 km box is superposed on top of a map of the Amchitka region in Figure 2.3.

The velocity structure for the model was derived from two sources. Shallow structure for the area from marine seismic profiles was reviewed by Lambert, *et al.* (1969). They present a model with maximum crustal thickness between the island and the trench (about 40 km), and thinning crust behind the arc to merge with a normal oceanic crust. We chose the oceanic PREM model

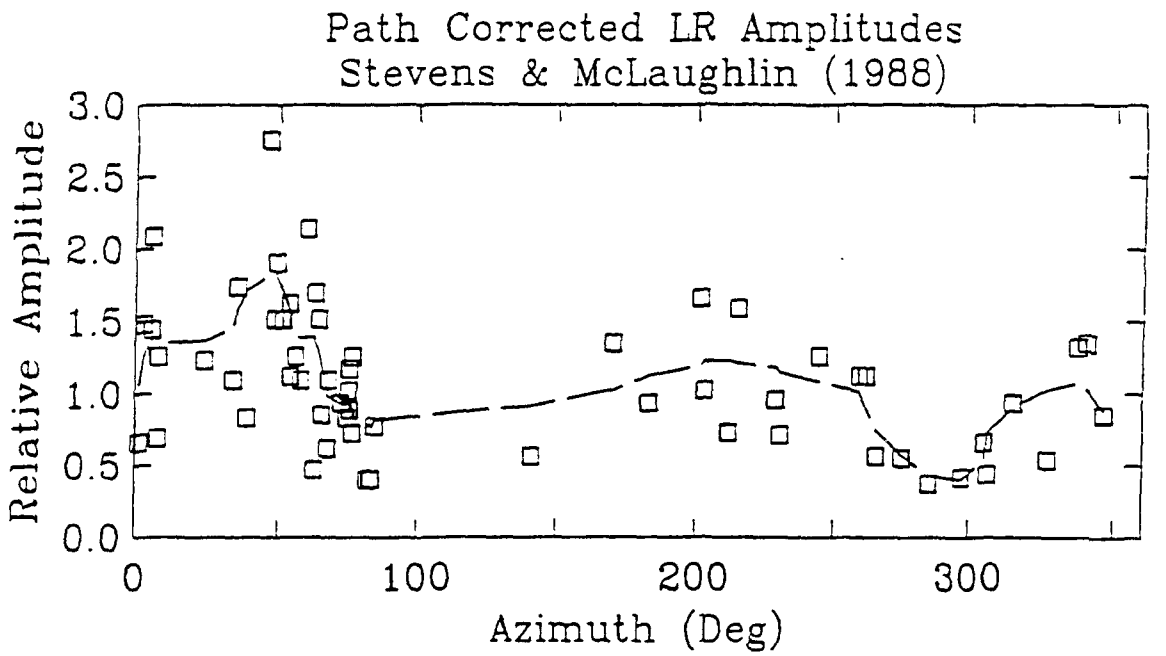

Figure 2.1. Path-corrected long-period Rayleigh-wave (LR) amplitudes from Stevens and McLaughlin (1988) for explosions LONGSHOT, MILROW, and CANNIKIN located at the Amchitka test site. Note the trend from large amplitudes between 40 and 60 degrees to small amplitudes between 60 and 90 degrees. A nonparametric smoother has been applied to the data (dashed line).

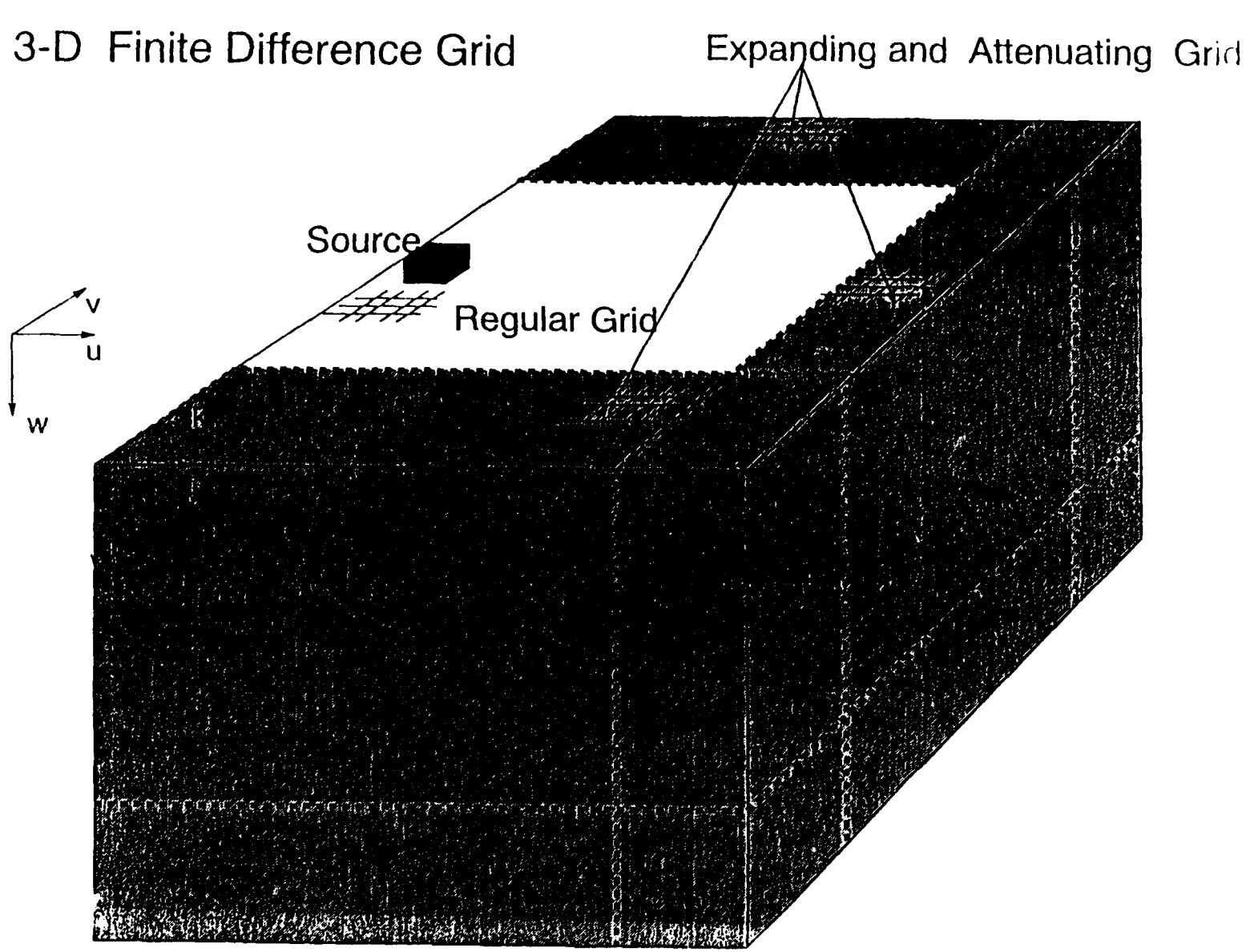

Figure 2.2.. The 3D finite difference grid was oriented with the v axis aligned north, u axis east and z axis down. A reflection symmetry boundary condition was used on the u = 0 plane taking advantage of the north-south reflection symmetry of the subduction zone. The inner grid had 6 km spacing and was 140x70x70. The outer portion of the grid had a progressively expanding spacing. The entire grid was 200x100x100. Numerical viscosity was used to damp reflections from the expanding grid. A 0.25 second time step was used.

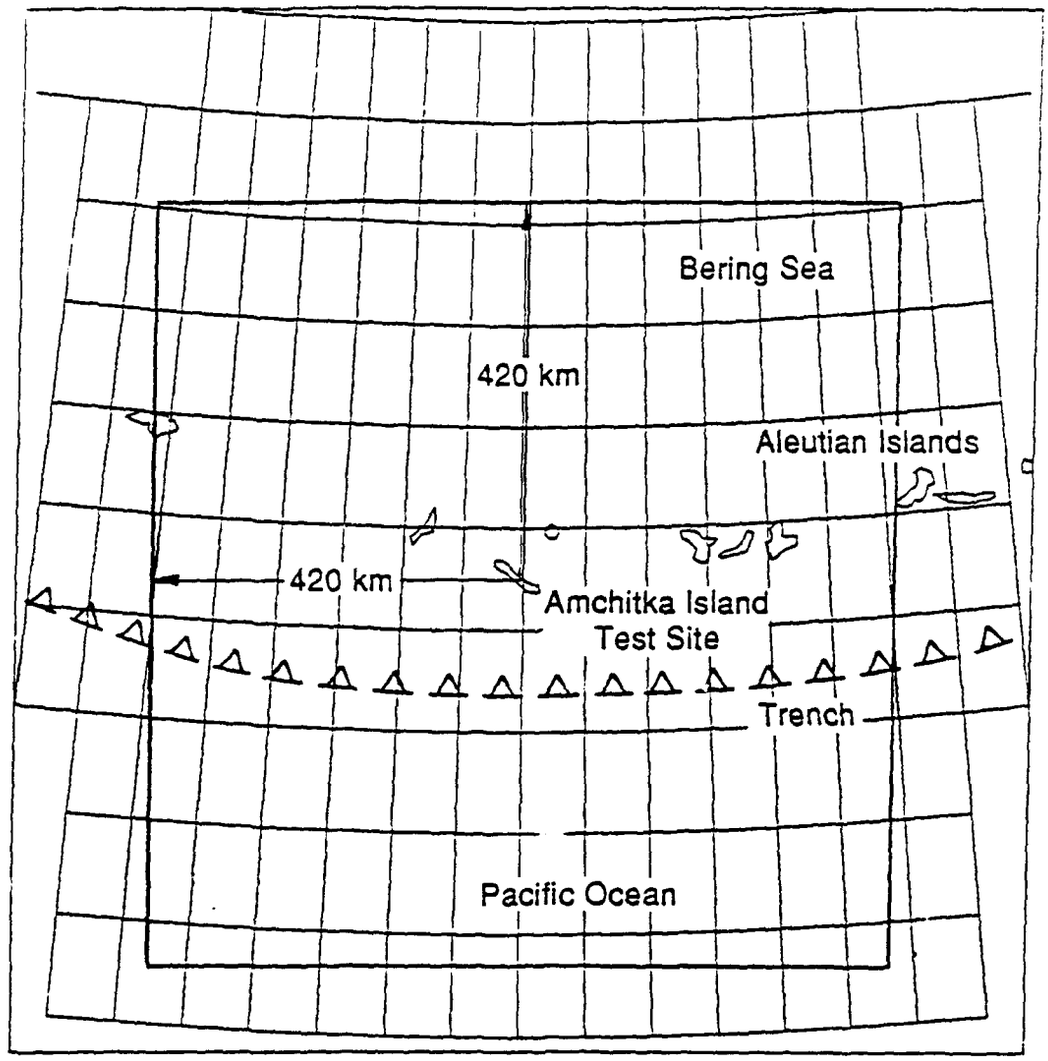

Figure 2.3. Map of region around Amchitka Island test site showing the approximate location of the trench axis and an 840 by 840 km box representing the finite difference grid used in the simulations.

north and south of the subduction zone as the limiting far-field velocity model. The mantle velocity from the spherically symmetric PREM model (Dziewonski and Anderson, 1983) was perturbed in accordance with a thermal model for the subducting lithosphere from Boyd and Creager (1991). The oceanic water layer was not included in the 3D calculations. The effect of the island/ocean interface was instead modeled in a separate series of 2D axisymmetric finite difference simulations (see Section 3 of this report and Stevens, *et al.*, 1990).

Two 3D linear elastic finite difference calculations were performed. In the first calculation, curvature of the Aleutian arc was ignored and the source was at location #1 indicated in Figure 2.4. In the second calculation, curvature of the subduction zone structure was included and the source location is indicated by #2 in Figure 2.4. Locations #1 and #2 bracket the location of Amchitka Island in the subduction zone structure with #1 closest to the approximate position of the island. A comparison of the two calculations shows similarities in the azimuthal effects, but the details of the final results are sensitive to the location of the source in the model and some model details. Some aspects of the velocity model are poorly controlled, such as the detailed thickness of the crust and the low velocity accretion zone north of the trench. For this reason, results are best considered as indicative of the magnitude and qualitative character of the probable effects of the subduction zone upon wave propagation.

Analysis procedures applied to the finite difference simulations included animated snap-shots of the displacement field at selected times, narrow band filter amplitude estimation, group and phase velocity estimation, and frequency-wavenumber analysis.

Animated snap-shots of the displacement field were resolved into vertical, radial, and transverse components in order to visualize the wave propagation. A color video of the evolving wavefield proved to be very helpful for visualizing the wave propagation and identifying areas for more detailed quantitative study.

Two snap-shots are shown in Figures 2.5A and 2.5B. The asymmetries in group velocity and amplitude are clearly evident from these figures. The structure to the east of the source along the strike of the structure is slower in the

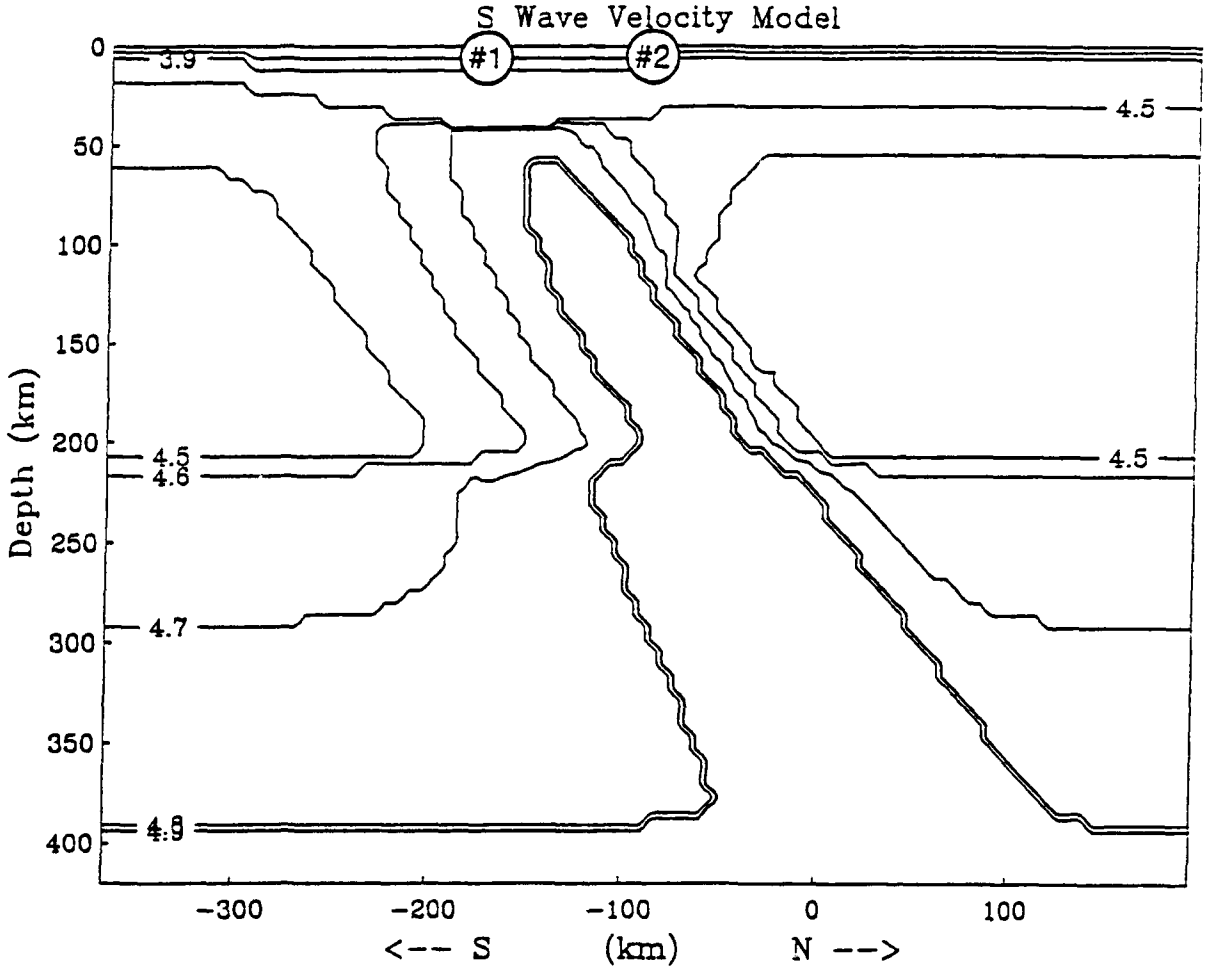

Figure 2.4. Contours of the S-wave velocity field along the north-south vertical plane. The model is based on Boyd and Craeger (1990) and Lambert, *et al* (1970). Two simulations were conducted, with an explosive source at #1 and #2 indicated in the figure.

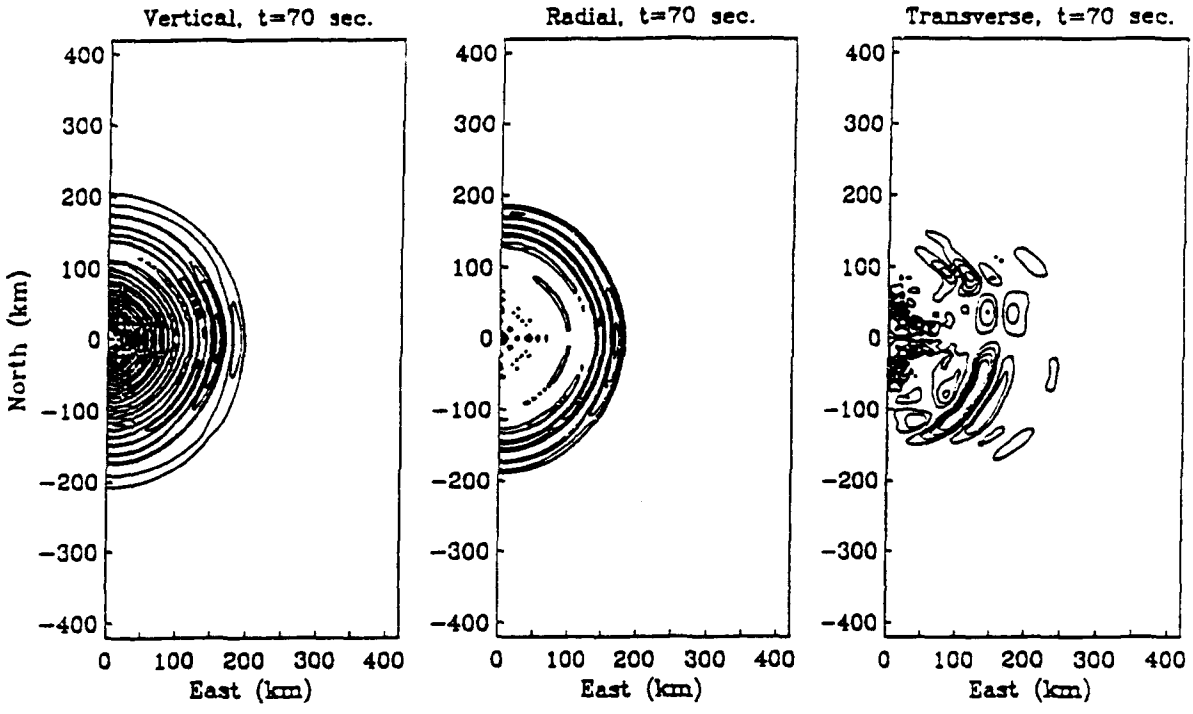

Figure 2.5A. Contours of displacement amplitude of the vertical, radial, and transverse components of motion on the free-surface of the finite difference grid at time t = 70 seconds. The motion is dominated by the fundamental Rayleigh wave on the vertical and radial components. Note the transverse motion beginning to form behind the Rayleigh wave southeast and northeast of the source. Simulation 3D#1.

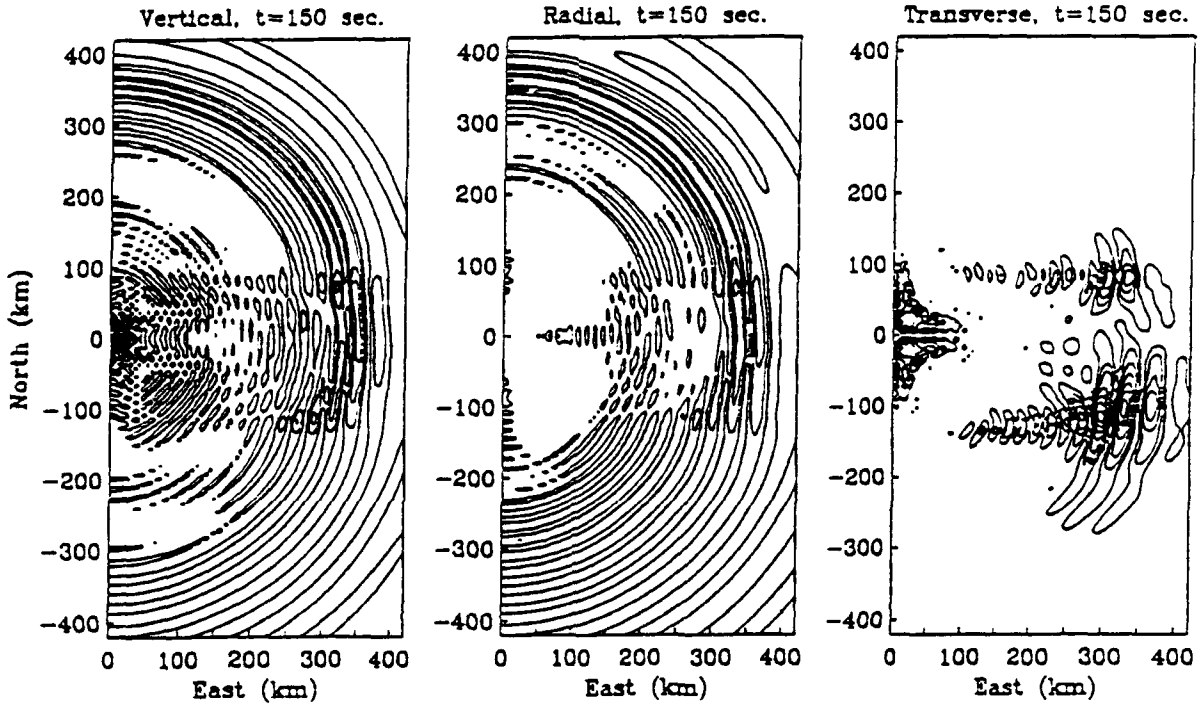

Figure 2.5B. Contours of displacement amplitude of the vertical, radial, and transverse components of motion on the free-surface of the finite difference grid at time t = 150 seconds. Rayleigh wave motion is both stronger and delayed to the east along the axis of the subduction zone. Love wave motion southeast and northeast of the source is overtaking the Rayleigh wave motion. Simulation 3D#1.

20-30 second period range because of the low velocity sediments and thick crust along the trench axis. Consequently, there exists a narrow low-velocity zone that forms a channel for surface waves. Refraction around this channel causes focusing of surface wave amplitudes along the axis of the channel and defocusing in regions immediately off-axis (north and south) of the channel.

The snap-shots (Figure 2.5) of the transverse component of motion show a growing transverse wave that develops along the north and south margins of the low velocity channel. The transverse amplitudes are about 1/4 the amplitude of the radial Rayleigh wave and appear to be associated with the passage of the Rayleigh wave along the edges of the low-velocity channel. Frequency-wavenumber spectra were used to confirm the presence of Love wave type motion.

In order to show the details of the surface wave amplitude anomalies across the surface of the grid, each vertical seismogram on the grid surface was narrow band filtered and the Rayleigh wave amplitude was estimated. Examples of these amplitudes are contoured in Figures 2.6 and 2.7. The Amplitude contours show the effects of both normal geometric attenuation and azimuthal variation from the 3D propagation.

To compute Rayleigh amplitudes at teleseismic distances, we developed a Fresnel-Kirchoff integral procedure to propagate surface waves to teleseismic distances and account for diffraction of the wavefront. This method assumes that the surface waves propagate from the edge of the 3D grid into a laterally homogeneous earth structure to receivers far away without additional complication. This assumption allows us to calculate the effects of far-field diffraction from the near-source scattering modeled by the 3D finite difference grid.

The amplitude and phase of the free-surface seismograms at fixed distances from the source are plotted in Figures 2.8A and 2.8B for the two simulations. This information is utilized in the numerical integral to compute the far-field teleseismic surface wave amplitudes. The phase (delay-advance) of the wavefield as a function of azimuth at the integration distance, R, is just as

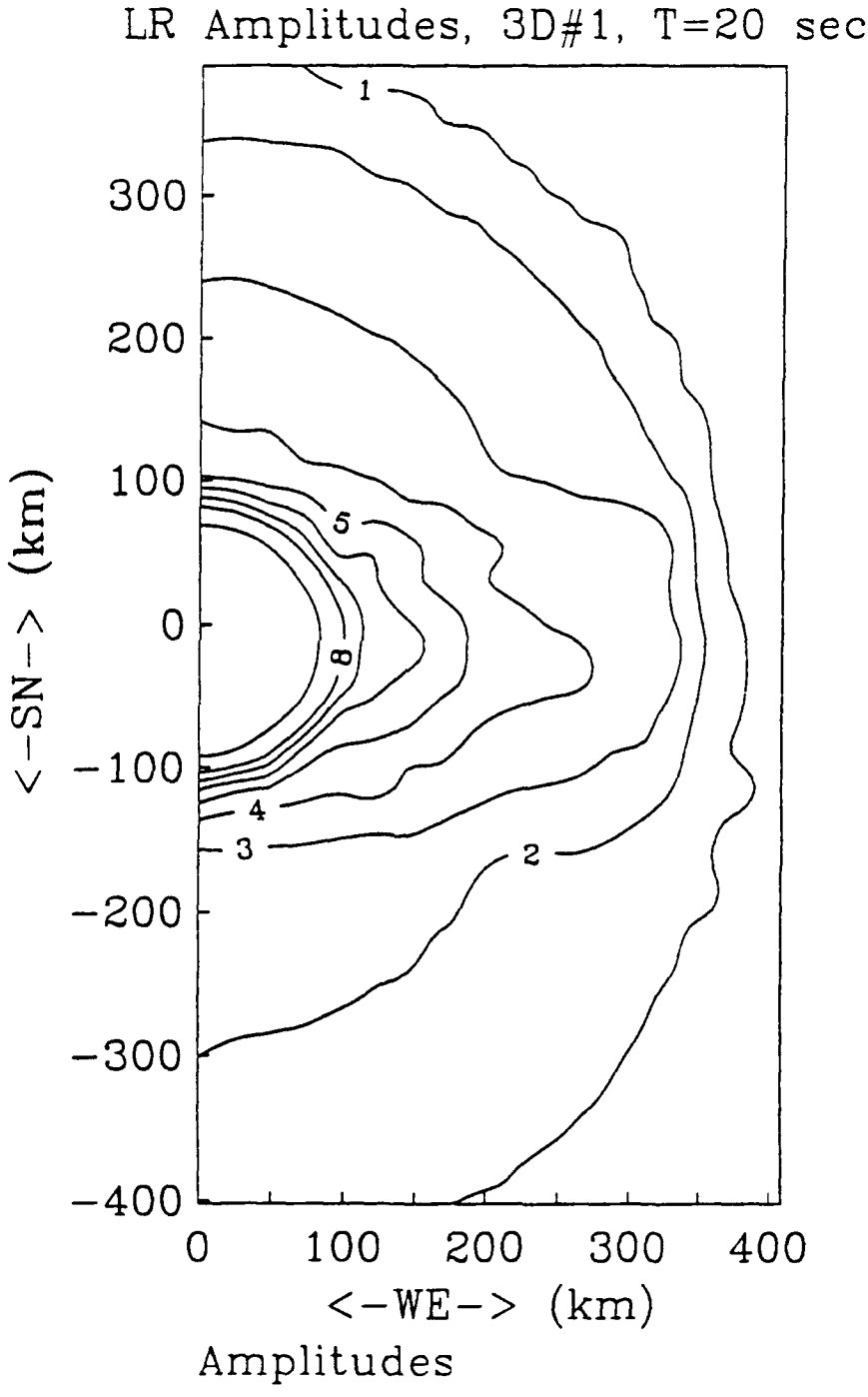

Figure 2.6. Contours of peak LR amplitude at 0.05 Hz from simulation 3D#1. Note the elongation of the contours in the east west direction.

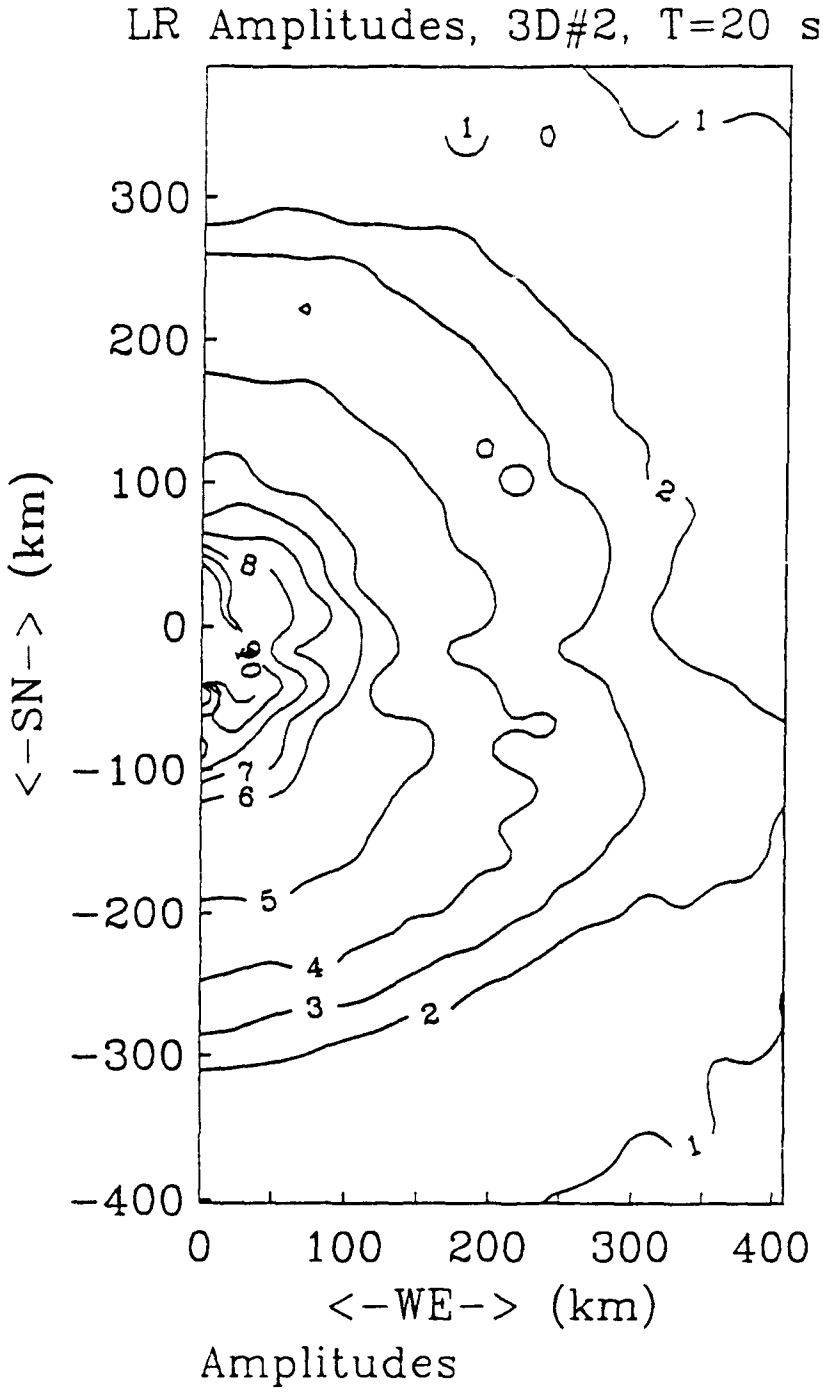

Figure 2.7. Contours of peak LR amplitude at 0.05 Hz from simulation 3D#2. Note the elongation of the contours in the east west direction.

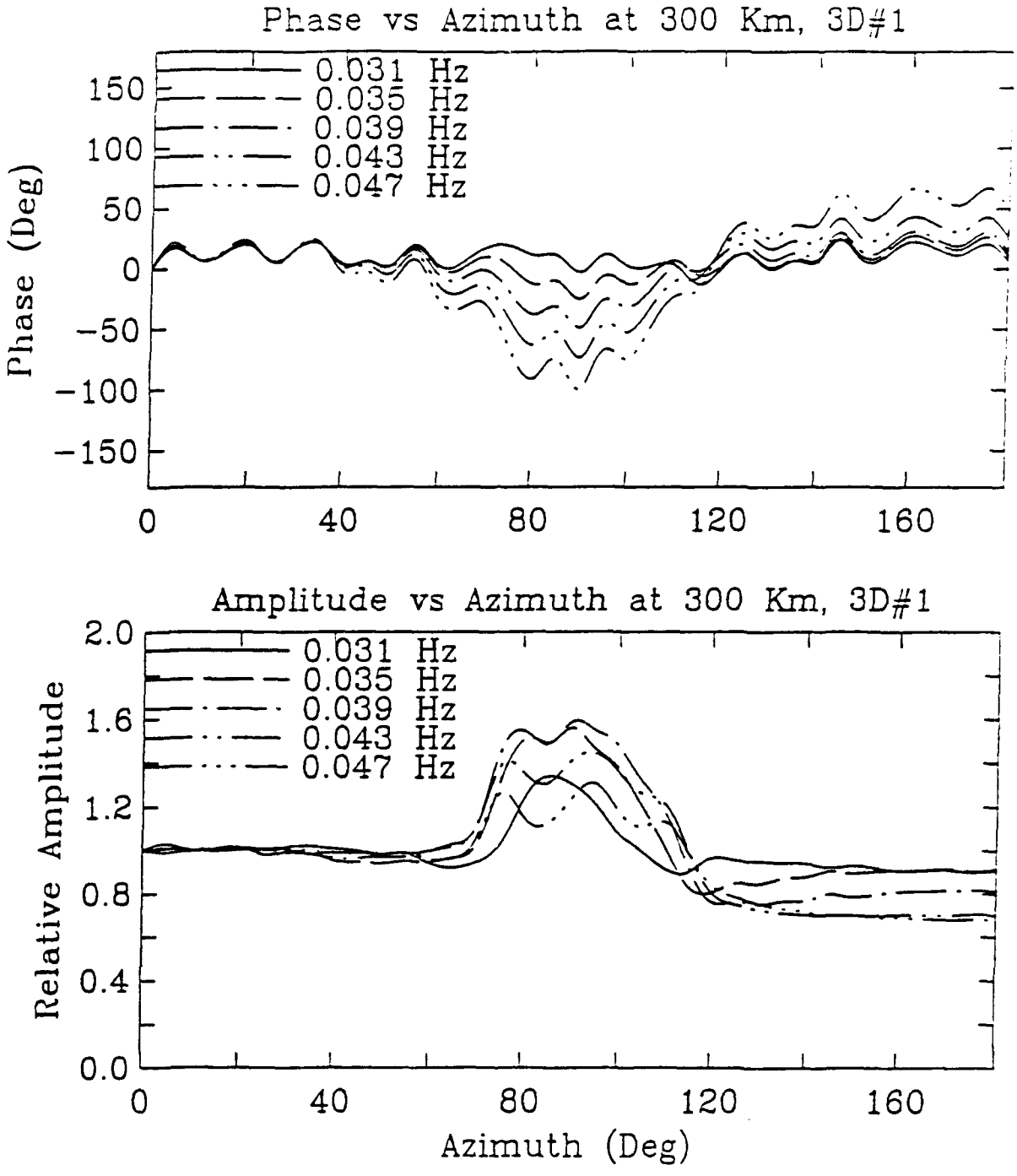

Figure 2.8A. The relative amplitude (bottom) and phase (top) for the Rayleigh wave at a distance of 300 km from the source in 3D simulation #1. Note the negative correlation between the large amplitude and phase (delayed) for azimuths to the east or west (90 degrees).

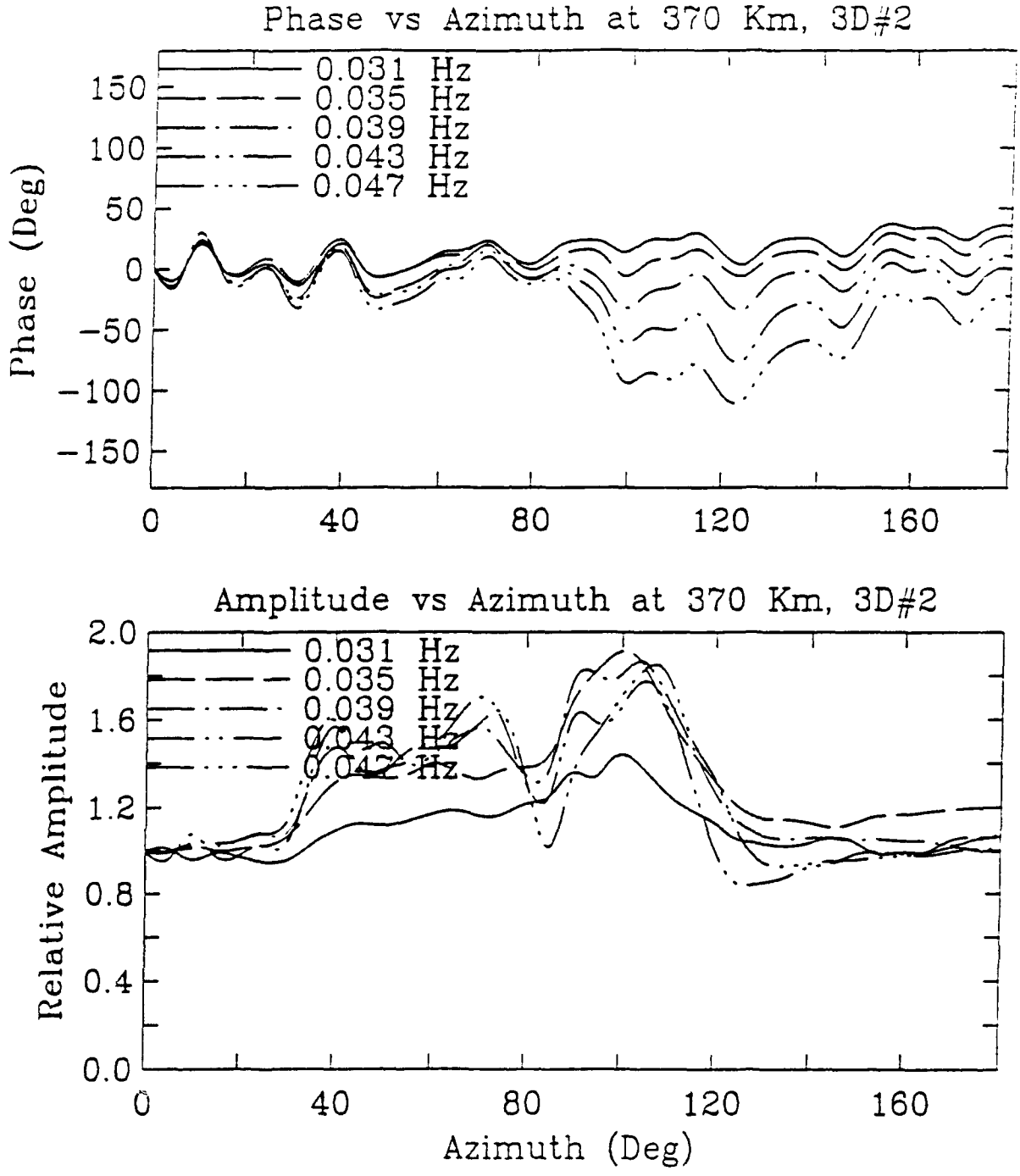

Figure 2.8B. The relative amplitude (bottom) and phase (top) for the Rayleigh wave at a distance of 370 km from the source in 3D simulation #2.

important as the amplitude dependence in the final amplitude at the far-field receiver.

Note the negative correlation between amplitude and phase for simulation 3D#1 in Figure 2.8A. This suggests that focusing/defocusing is largely responsible for the amplitude pattern at this distance from the source. Note also that for both simulations the amplitude patterns are similar at different frequencies while the detailed patterns are frequency dependent. Figures 2.9A and 2.9B plot the far-field relative amplitude as a function of amplitude and frequency. Although the patterns are frequency dependent, the different frequencies share some common patterns. The average relative pattern from 32 to 20 seconds period is shown in the upper frame of Figures 2.9A and B.

The far field radiation patterns shown in Figures 2.9A and 2.9B appear quite dissimilar at first glance, but in fact can both be characterized as having increased ampitudes with a maximum of about a factor of 1.5 to the east relative to the north and south, with a rapidly varying complex diffraction pattern superimposed on top of this slowly varying pattern. The effect of propagating the near field Rayleigh wave radiation to the far field is to spread out the amplitude increase which is concentrated in the east within the grid over a wider range of azimuths, and to cause some complex structure in the radiation patterns that is sensitive to the details of the model.

The Rayleigh wave observations from the Amchitka explosions (Figure 2.1), showed a very rapid decrease over a small range of azimuths that can be partially, but not entirely explained by tectonic strain release. The three-dimensional simulations do not reproduce this effect over the observed azimuthal ranges, however they do produce amplitude variations of as much as a factor of 2 over very small azimuthal ranges. These variations are sufficiently sensitive to the details of the model to suggest that the observed anomalies are diffraction effects similar to those predicted by the three-dimensional calculation.

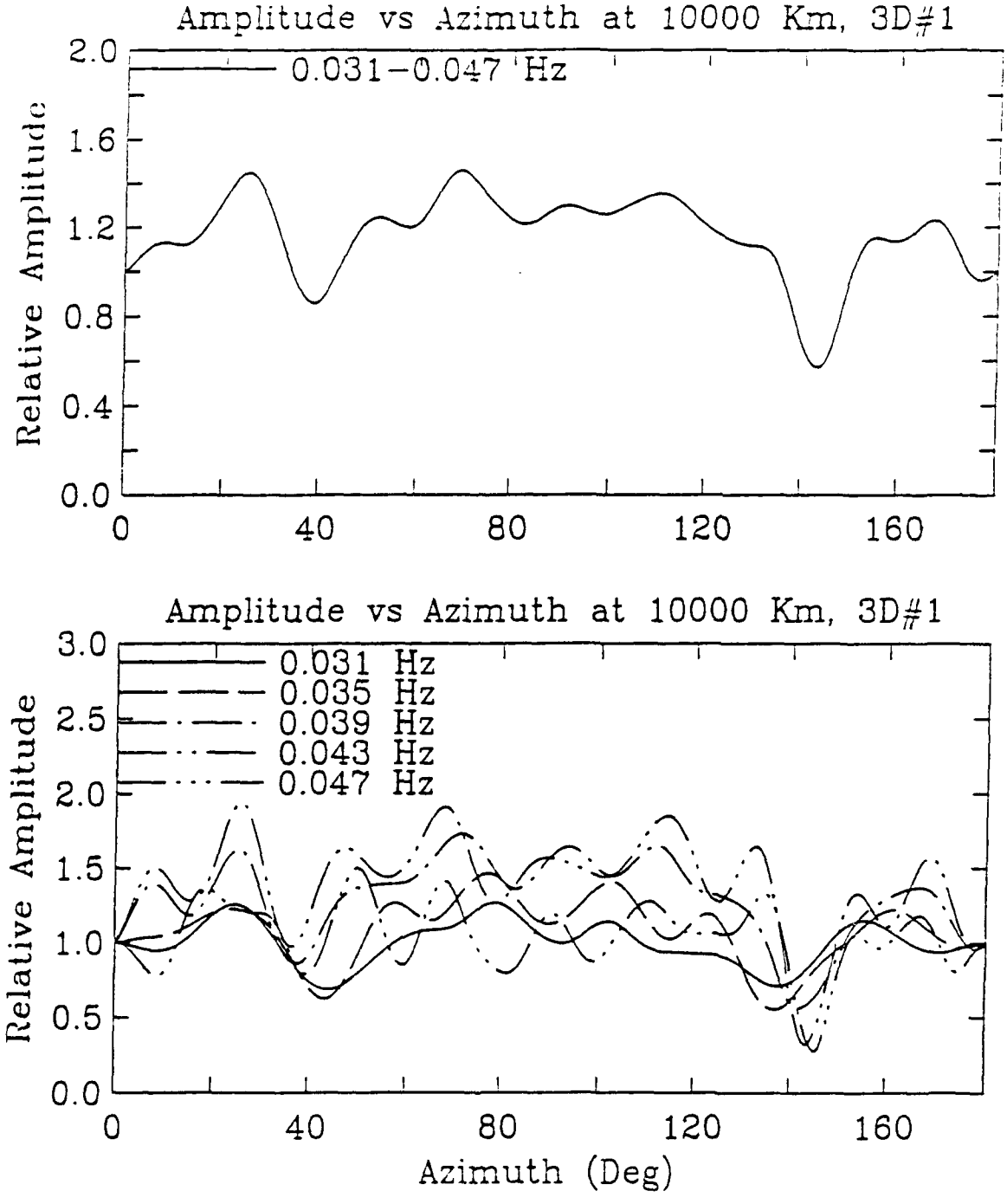

Figure 2.9A. Predicted teleseismic amplitudes from 3D simulation #1 as a function of azimuth using the Fresnel-Kirchoff integral to account for diffraction effects in the far-field. The average relative amplitude from 32 to 20 seconds period is at the top.

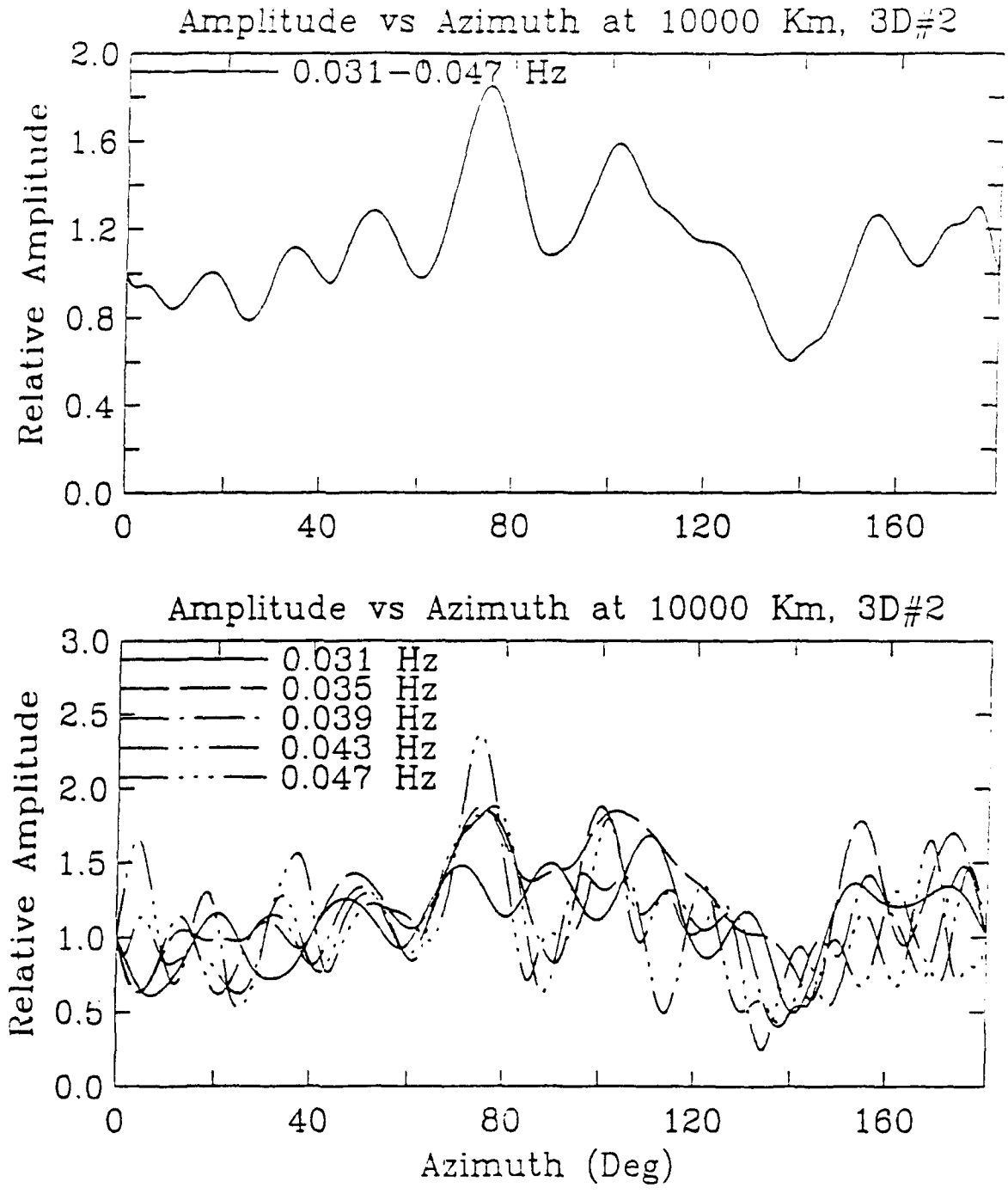

Figure 2.9B. Predicted teleseismic amplitudes from 3D simulation #2 as a function of azimuth using the Fresnel-Kirchoff integral to account for diffraction effects in the far-field. The average relative amplitude from 32 to 20 seconds period is at the top.

3. The Excitation of Surface Waves by an Explosion on an Island.

The Amchitka and Mururoa test sites are unique in that they are located on islands in the Pacific Ocean. Estimation of explosion yields using surface waves from explosions at these sites requires an understanding of the effect of the island/ocean transition on surface wave generation. There is evidence of anomalous surface waves from the Amchitka explosions. The surface wave amplitudes of the Amchitka explosion Milrow, for example, were significantly smaller than the surface wave amplitudes for NTS explosions Boxcar, Benham, and Handley, all of which had similar yields (von Seggern, 1978; Stevens, 1986b). Also, as discussed in the previous chapter, a very strong radiation pattern was observed from all three Amchitka explosions, and Love waves were observed from explosions and collapses.

In this study, we look at the effect of the island/ocean interface on the generation of surface waves by an explosion. We have also extended the study to other cases of interest by using "island" in a generic sense to mean a source region of higher velocities than the surrounding regions. We have performed three sets of calculations: first with the island surrounded by air; second with the island surrounded by water; and third with the island surrounded by a low velocity solid. The calculations therefore apply not only to an explosion on an island, but also to an explosion in a mountain, or to an explosion in a high velocity intrusion such as a salt plug. We look in particular at the effect of the size of the island and the depth of the ocean on the surface wave amplitudes. We find that the surface wave amplitudes can be reduced significantly by the presence of a near vertical boundary near the source.

The calculations were performed with the two-dimensional finite difference code TRES-2D running on a CRAY 2 supercomputer. We used a uniform grid spacing of 1.5 km, which is designed to allow accurate resolution of surface waves in the 10-50 second period band. A schematic diagram of the geometry used in the calculations is shown in Figure 3.1. The explosion was modeled as a pressure pulse with a fixed moment applied to the first two vertical zones at the axisymmetric origin adjacent to the free surface. Calculations were

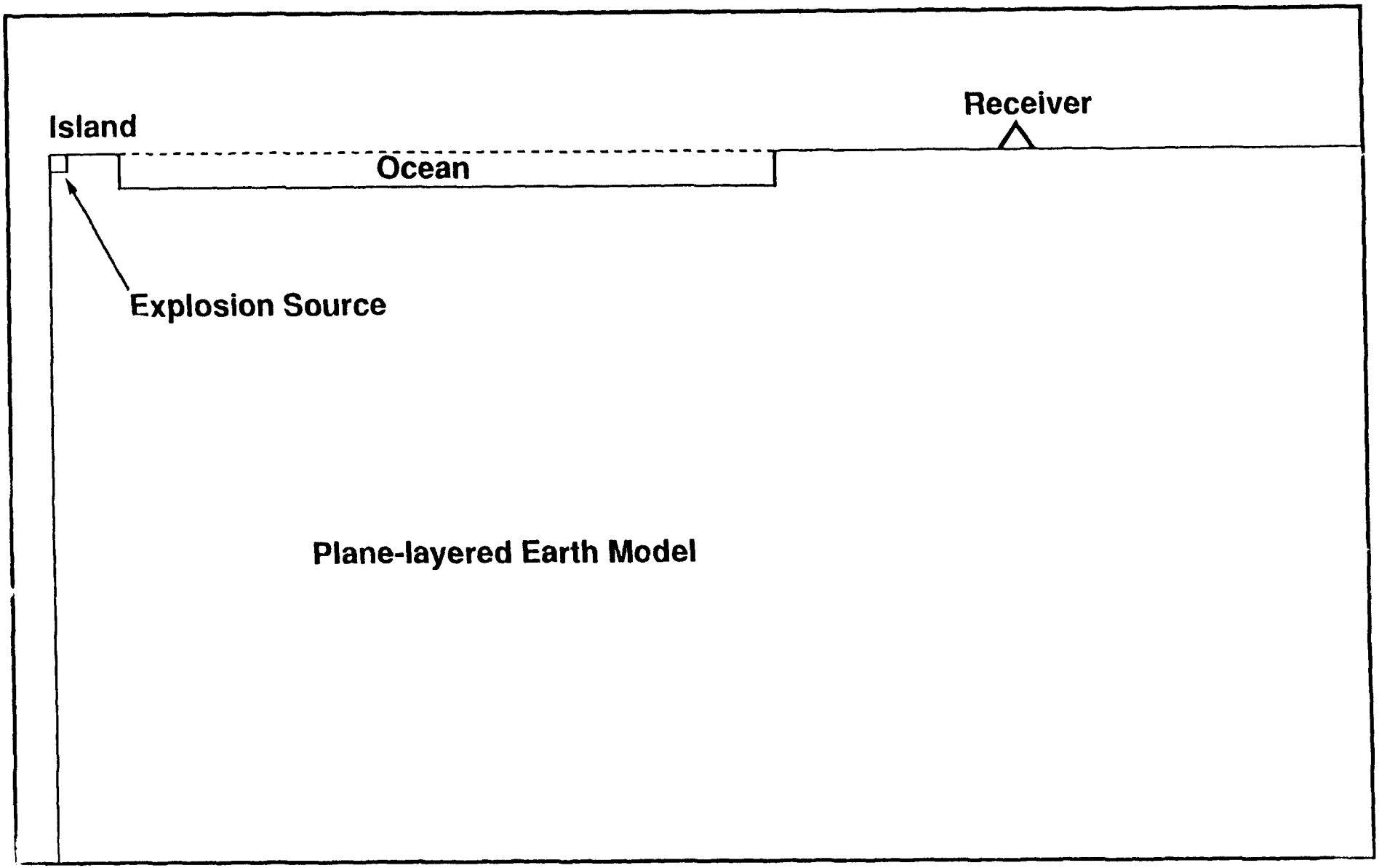

Figure 3.1. *Geometry of the two-dimensional axisymmetric finite difference calculations.* The explosion source is located just below the surface at the origin. The ocean extends to a distance of 354 km from the origin, and the receiver is located 390 km from the origin. The set of calculations includes ocean depths of 3 km and 6 km, and island radii ranging from 3 km to 24 km.

performed for island radii ranging from 3 km to 24 km, and for ocean depths of 3 km and 6 km.

The "ocean" in this model is a region with material properties different from the background model. The background model is a plane-layered model, and is equivalent to a north-south cross-section near the Amchitka test site in the three dimensional model of McLaughlin, *et al.* (1991). One calculation was performed as a reference using the background structure without the ocean. Three sets of calculations were performed with different material models in the "ocean." In the first set of calculations, the ocean was filled with water using standard water density and compressional velocity. In the second set of calculations, a free surface boundary condition was used on the bottom and sides of the ocean, thus simulating air or vacuum in the "ocean." In the third set of calculations, the ocean was filled with a solid with a compressional velocity of 2.4 km/sec, a shear velocity of 1.3 m/sec, and a density of 1.9 g/cm^3. These values are typical of the volcanic tuffs found at the Nevada Test Site. This model therefore simulates a high velocity intrusion into a lower velocity medium.

The amplitude and phase of the surface waves at the receiver were recovered by narrow band filtering and phase-matched filtering as described by Stevens (1986a). In Figure 3.2, we show the spectra between .01 and 0.1 Hz for the uniform backgound structure, and for the water, air, and solid filled ocean cases with an island radius of 24 km, and an ocean depth of 3 km. For this small aspect ratio (aspect ratio is defined here to be the ratio of the island height to the island radius), the island structure has little effect on the surface wave amplitudes. The material property differences cause some variation in spectral amplitude at higher frequencies, but at frequencies less than 0.05 Hz, there is very little differences between the surface wave amplitudes for any of the four structures.

In Figure 3.3, we show the surface wave amplitudes for an island radius of 6 km, and an ocean depth of 6 km. In this case the amplitudes are very strongly reduced for all three ocean types. At 25 second period (0.04 Hz), the amplitudes are reduced relative to the uniform case by factors of 2, 6, and 20 for the solid, water, and air filled ocean cases, respectively. In Figures 3.4, 3.5, and 3.6, we show the 25 second amplitude as a function of the aspect ratio of the

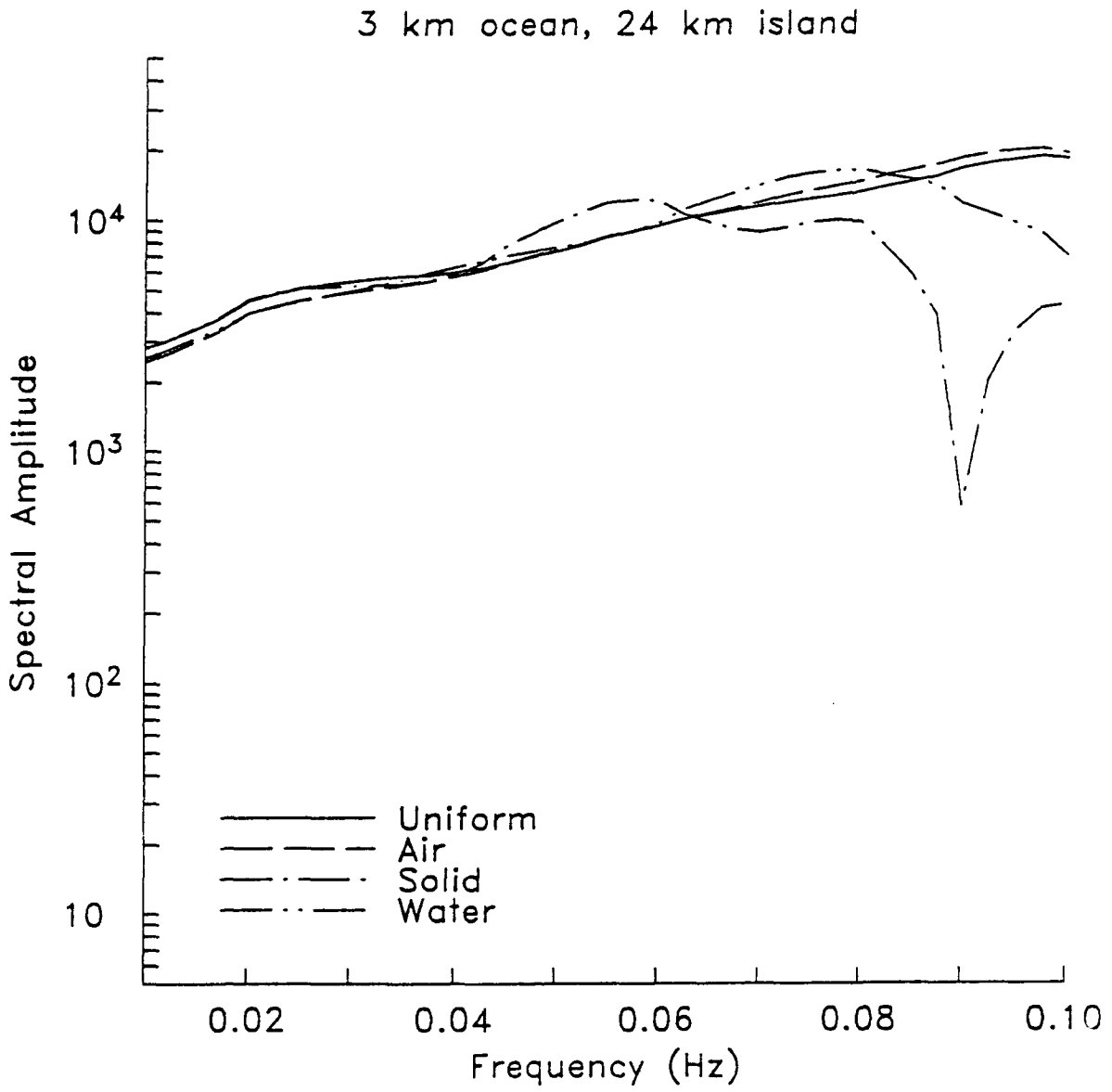

Figure 3.2. Spectra of surface waves recorded at 390 km from a 24 km radius island across the uniform background structure, and across an "ocean" filled with water, air, and a lower velocity solid. In each case, the "ocean" is 3 km deep. The "ocean" material has some effect on shorter period surface waves, but there is little difference between the three cases at periods greater than 20 seconds.

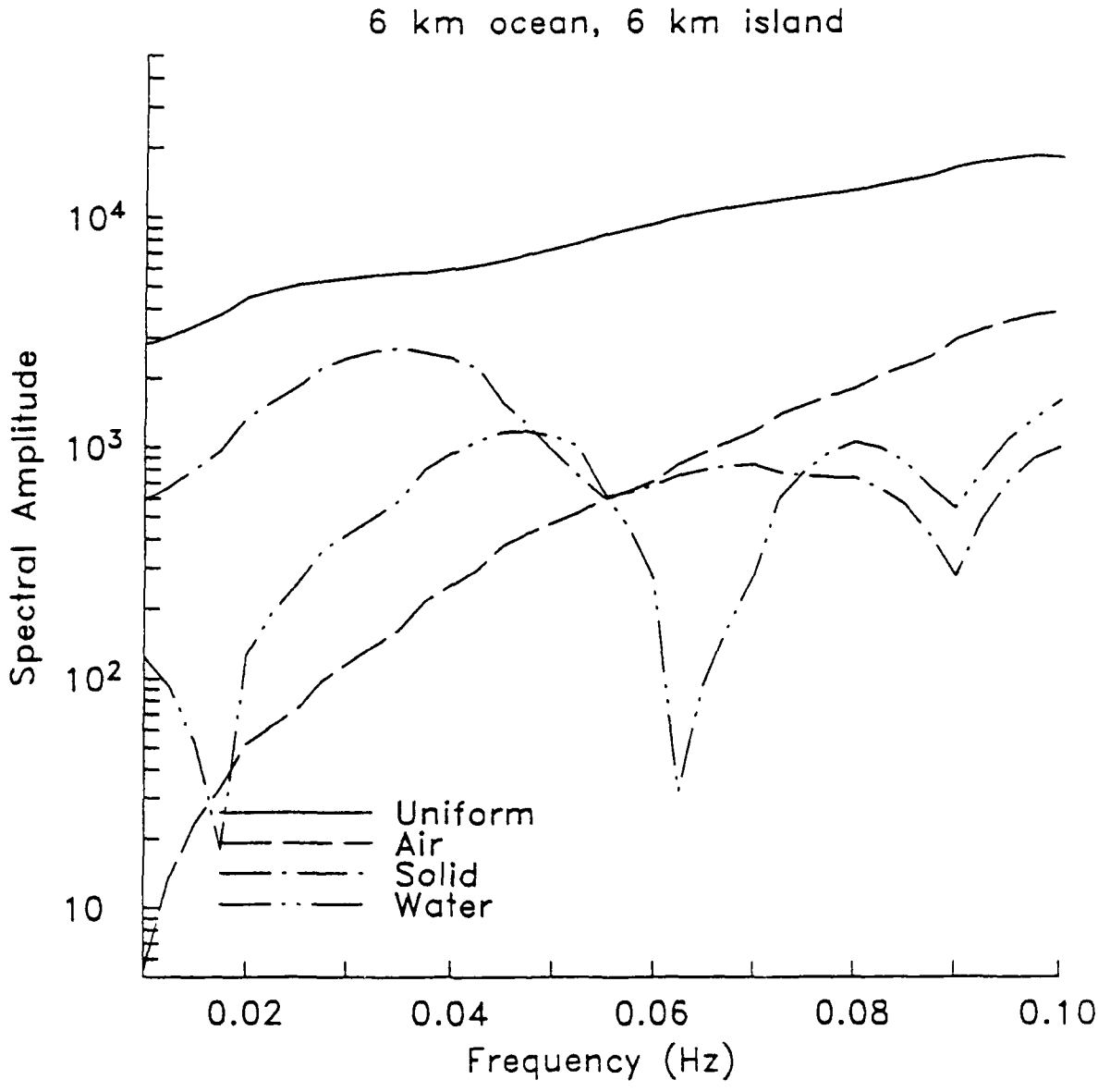

Figure 3.3. Spectra of surface waves recorded at 390 km from a 6 km radius island across a 6 km deep "ocean" of water, air, and solid. The surface wave amplitudes are sharply reduced at all frequencies in all cases.

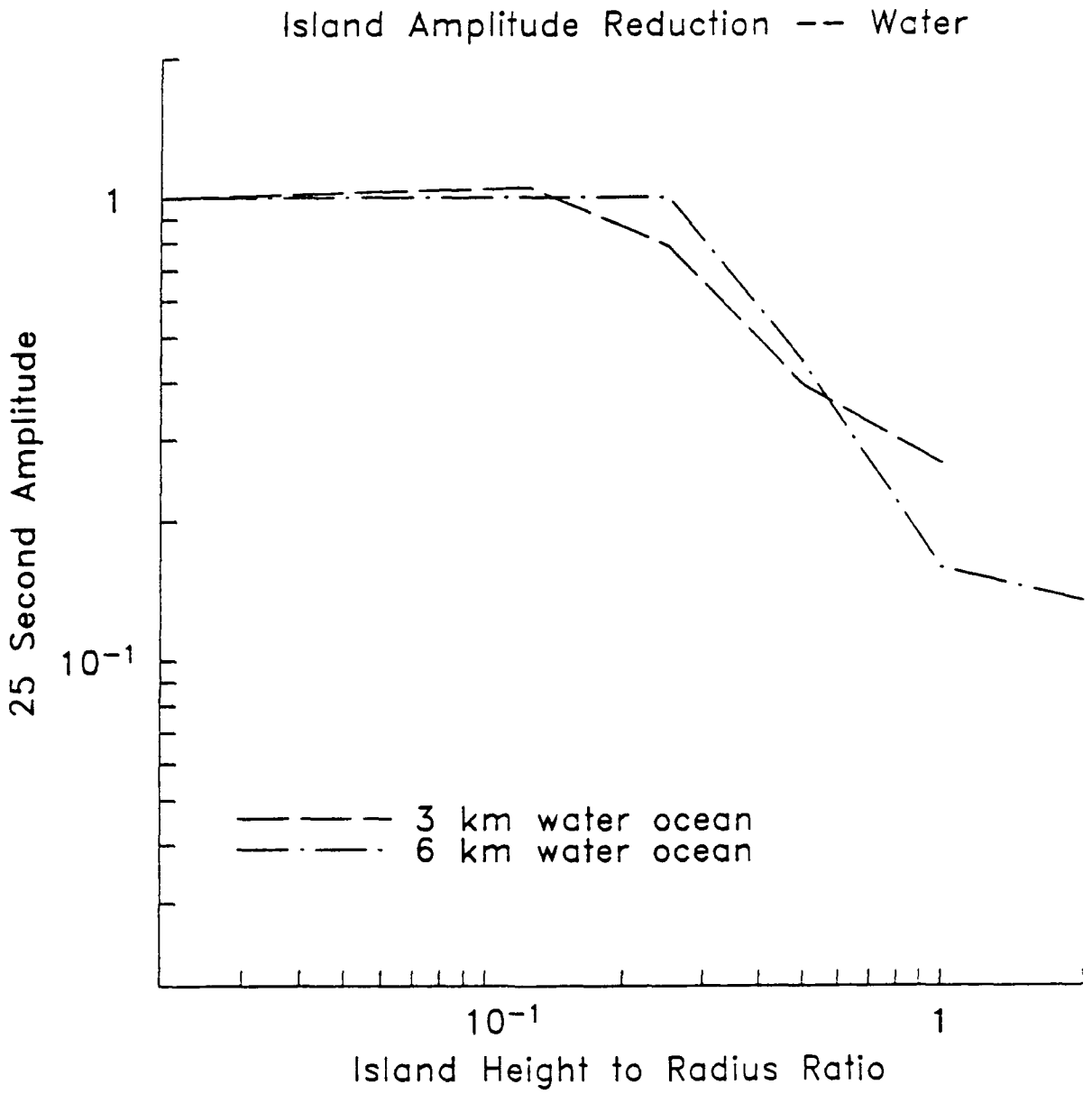

Figure 3.4. 25 second surface wave amplitude as a function of the island aspect ratio (ratio of island height to radius) for a water ocean.

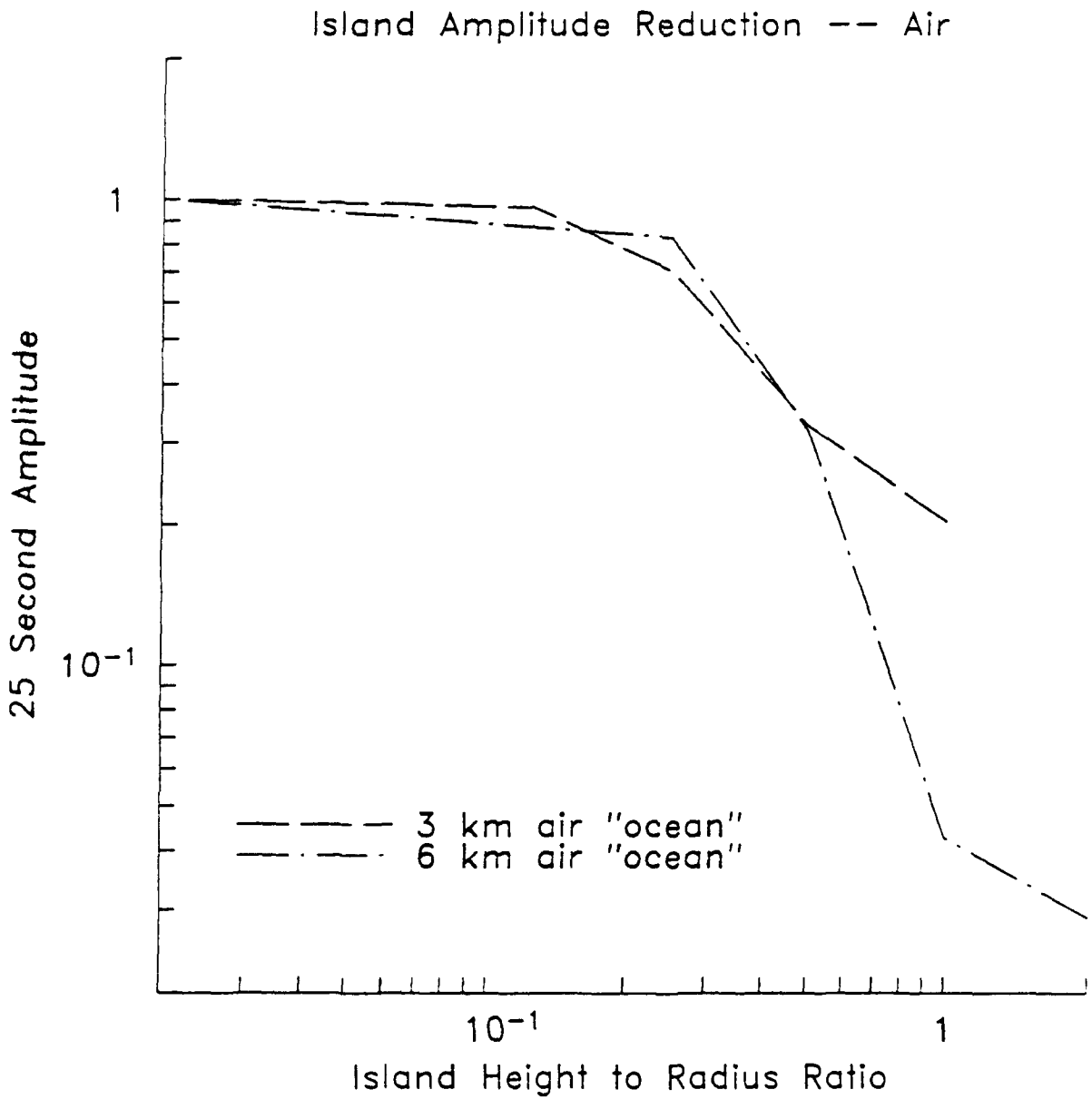

Figure 3.5. 25 second surface wave amplitude as a function of the aspect ratio for an air-filled "ocean".

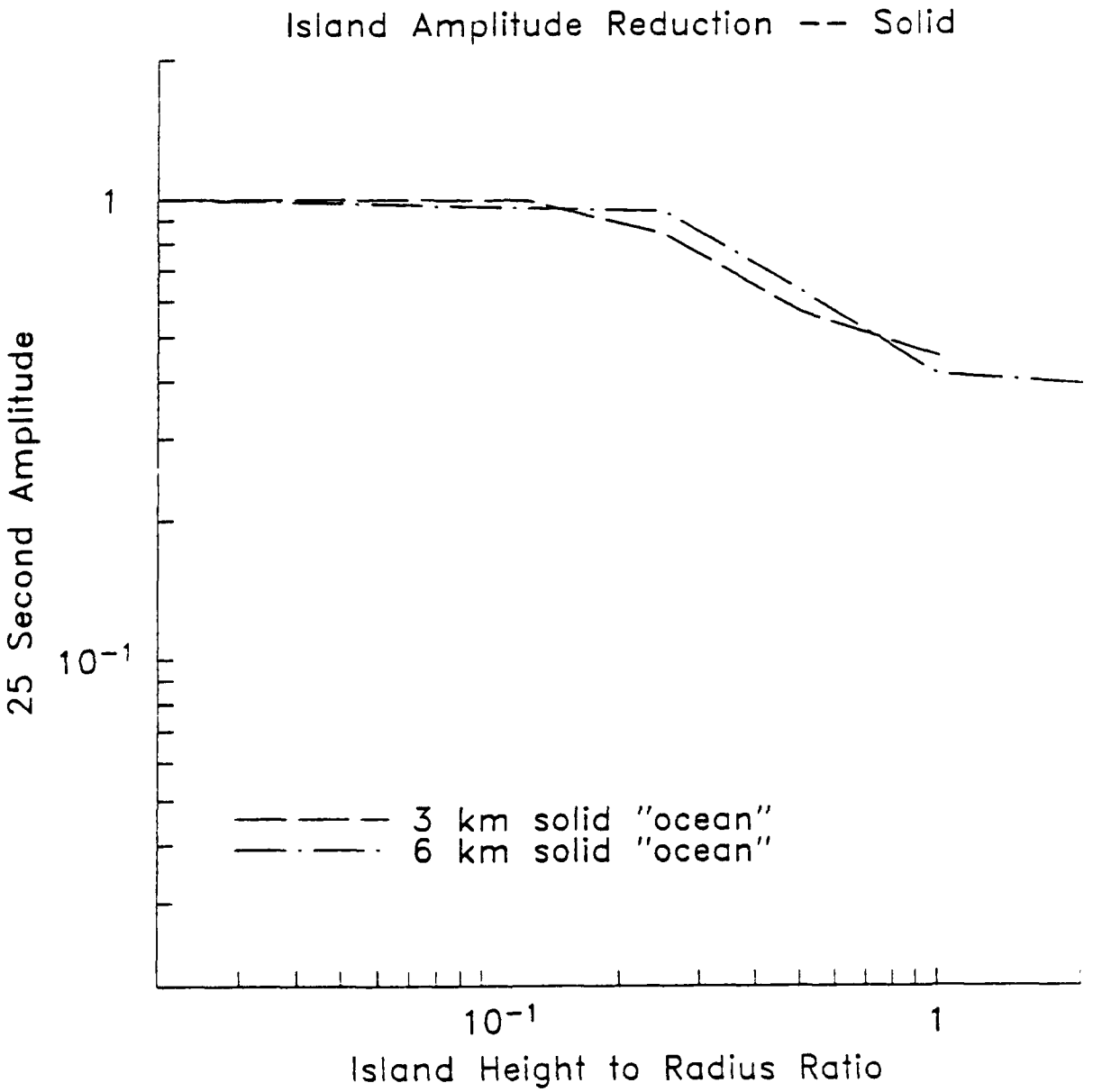

Figure 3.6. 25 second surface wave amplitude as a function of the aspect ratio for an "ocean" filled with a lower velocity solid.

island. In each case, the amplitude is reduced for aspect ratios greater than about 0.2, and the amplitudes are reduced by a factor of 2 at aspect ratios of 0.35, 0.4, and 0.7 for air, water, and solid, respectively. For the solid model the amplitude is reduced by a maximum of about a factor of 2.5, and the amplitude reduction can be much larger for the air and water cases.

The physical mechanism for the amplitude reduction is the relaxation of horizontal stress by the vertical boundary. For a shallow explosion source, surface waves are generated only by the horizontal stress components, since the free surface boundary condition relaxes the vertical component of stress. Adding a vertical boundary, however, relaxes the horizontal components also, making the explosion a very poor generator of surface waves in some cases.

In Figure 3.7, we show the bathymetry near the Amchitka and Mururoa test sites. The Amchitka bathymetry was derived by drawing a line southwest from the test site using maps from Olsen, *et al.* (1972). The Mururoa bathymetry was derived similarly by drawing a line to the northwest of the test site using maps from DMA (1983). For Amchitka, the aspect ratio is only about 0.05, so the amplitude reduction from the island structure at Amchitka is small. At Mururoa, however, the ocean drops off much more quickly away from the test site, and the aspect ratio of the island is approximately 0.25. Surface waves will therefore be reduced slightly at the Mururoa test site by this effect.

A final important question is the effect of topography and depth on surface wave generation. That is, will the predicted amplitude reduction discussed above vanish if the explosion is below the base of the mountain, or will the distortion of the local stress field continue to cause an amplitude reduction. The numerical tests described above used a grid too coarse to answer this question, so we performed a numerical reciprocal experiment in 2D plane strain. The geometry of this experiment is shown in Figure 3.8. A planar Rayleigh wave pulse is incident from the left upon a steep mountain with 45 degree slopes and height L = 12 units and radius of 16 (aspect ratio 0.75). The half space had a compressional velocity of 6 units/sec, and a shear velocity of 3.55 units/sec. Vertical displacements and dilatations are recorded at locations indicated on the figure. Incident displacement and dilatation are then used to normalize each synthetic seismogram to the incident pulse. The seismogram

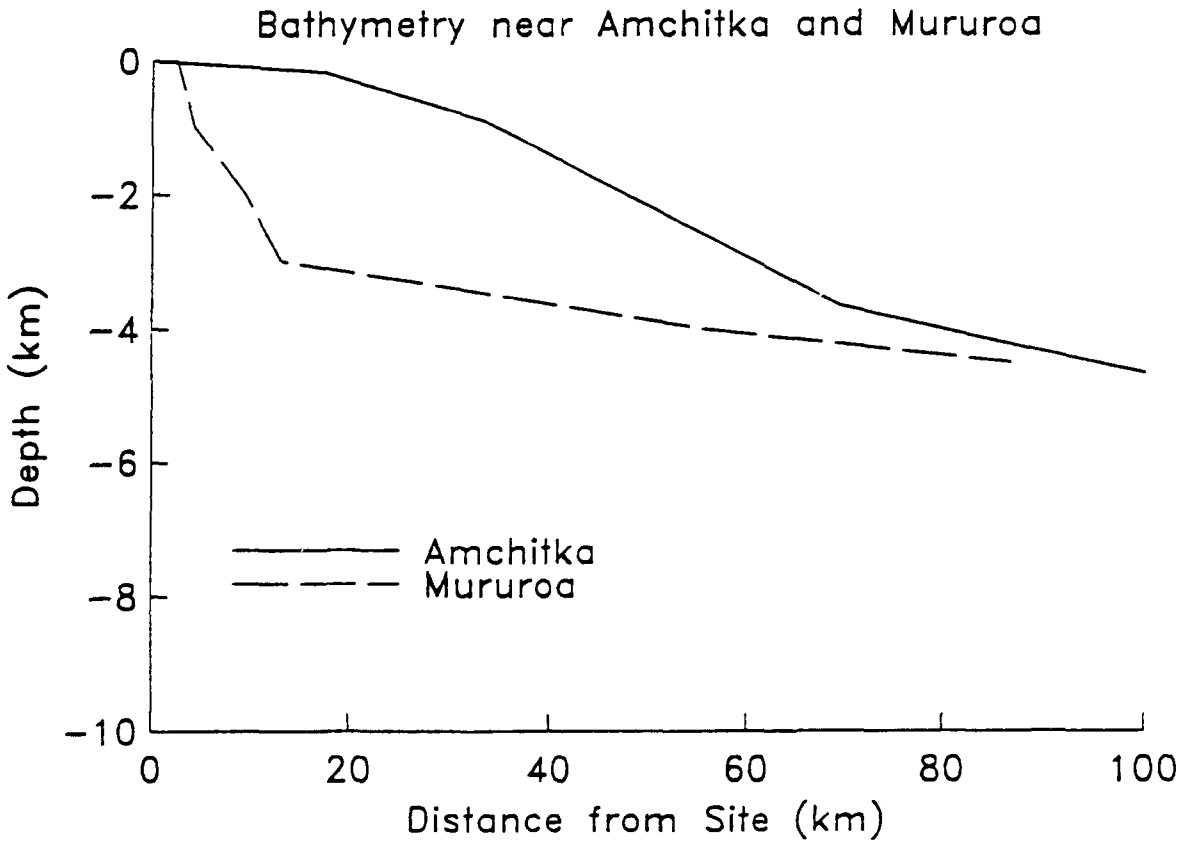

Figure 3.7. Bathymetry near the Amchitka and Mururoa test sites.

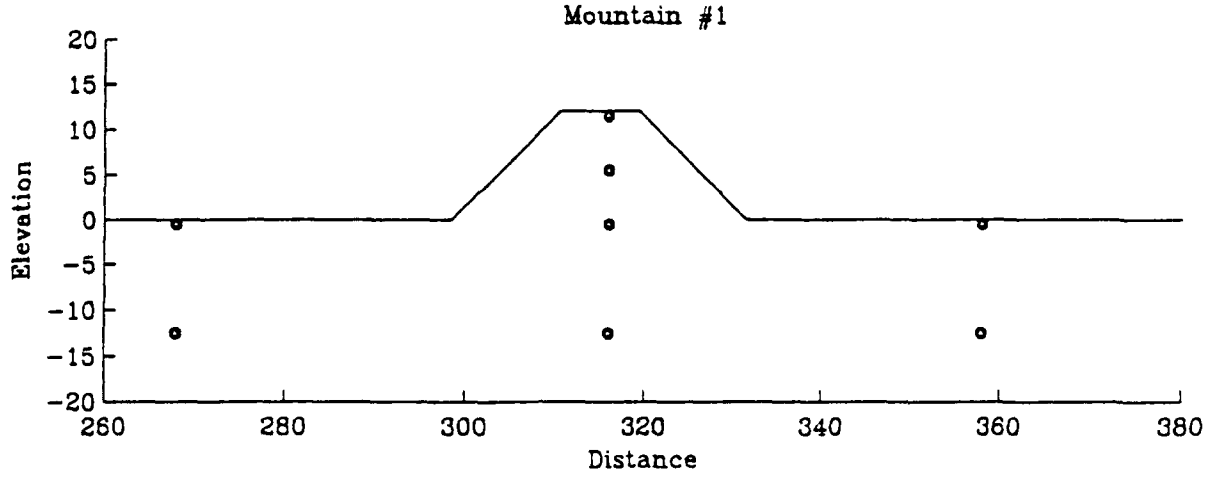

Figure 3.8. Geometry of the 2-D plane strain reciprocal experiment. The vertical displacements and dilatations due to an incident Rayleigh wave were measured at the locations shown. This is equivalent to measuring the far field Rayleigh wave generated by a vertical point force and explosion, respectively.

locations correspond to the top, middle, and bottom of the mountain as well as a location deep under the mountain (12 units) and a location on the far side of the mountain (transmitted) at two depths (deep and shallow).

By reciprocity the ratio of the recorded displacement to the incident Rayleigh wave vertical displacement is the equivalent to the far-field Rayleigh wave displacement from a vertical point source. Similarly, the ratio of the recorded dilatation to the incident Rayleigh wave is equivalent to the far-field Rayleigh wave from a dilatational source. Therefore, we can examine the relative far-field Rayleigh wave excitation from sources within and under the mountain. The effect of transmission through the mountain from source to receiver can be examined as well.

Figure 3.9 shows the spectral amplitude ratio of the vertical displacements to the incident Rayleigh wave displacement as a function of normalized wavenumber, $k' = \frac{2\pi fL}{c}$, where L = 12 units is the height of the mountain, c = 3.252 units/sec is the Rayleigh wave phase velocity, and f is frequency. This is the reciprocal problem of the Rayleigh wave generated by a point force at the locations shown. We consider $k' << 1$ to be the long period limit while $k' \sim 1$ corresponds to the resonances in the scattering problem. Note that the effect of a vertical point force at the top, middle, bottom, or deep under the mountain is not much different than a source to the side of the mountain with transmission through the mountain. Some amplitude is lost due to scattering but from $k' = 0.1$ to $k' = 1$, the effect is generally less than 30%. For $k' < 1$, the effect of the mountain for a vertical point force is comparable to the transmission through the mountain and less than 30%.

However, if we examine the problem of explosive sources at these locations, the results are quite different. Figure 3.10 shows spectral amplitude ratios for dilatational recordings at the respective source locations normalized to the incident Rayleigh wave dilatation. Note that a source deep under the mountain is much the same as a source to the side of the mountain with transmission through the mountain, and for $k' = 0.1$ the effect is less than 30%. However, the Rayleigh wave excitation from a source at the top of the mountain is reduced by nearly 90% at low frequencies. The deeper the source, under the

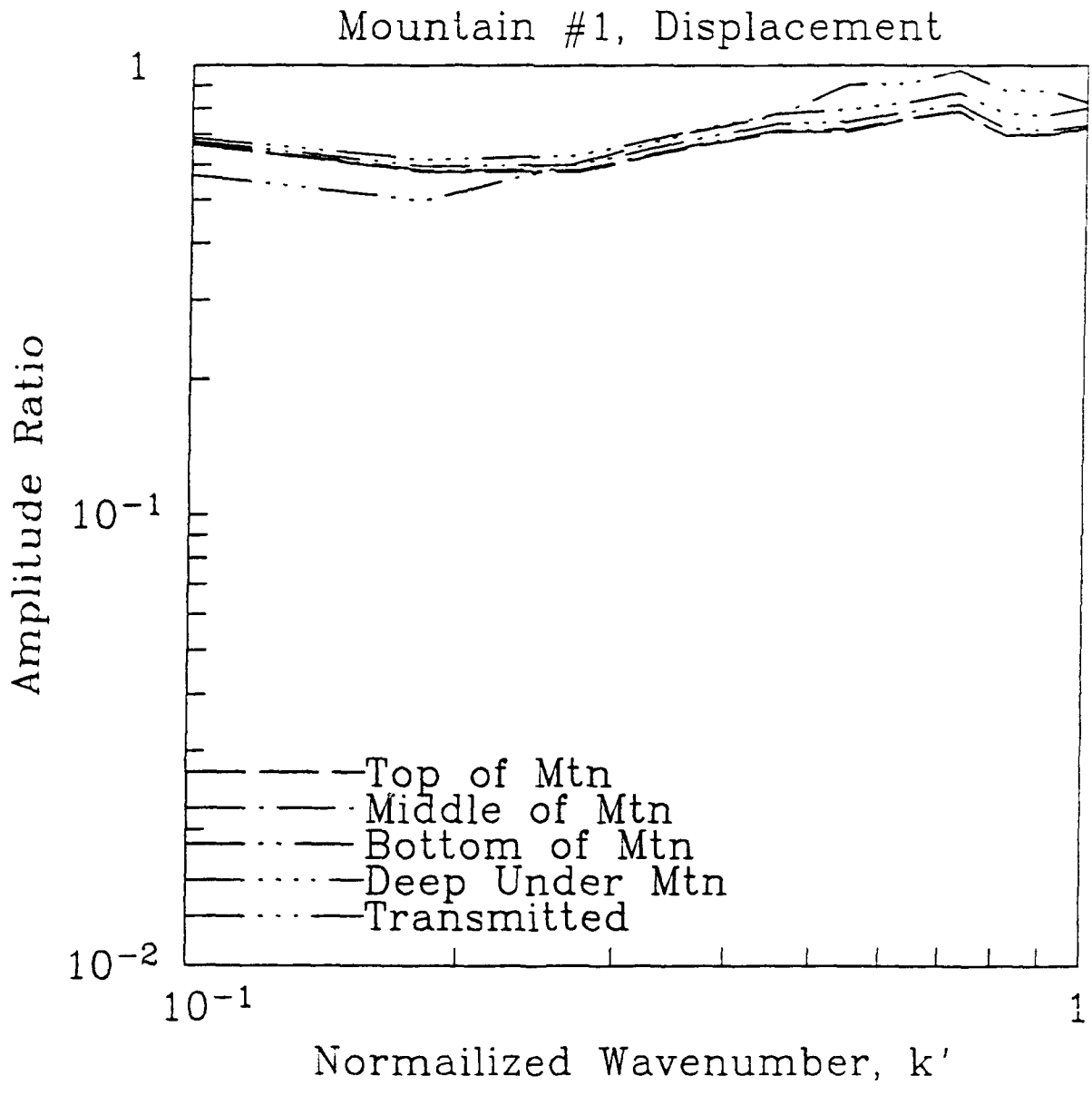

Figure 3.9. Spectral amplitude ratio of the vertical displacements to the incident Rayleigh wave displacement as a function of normalized wavenumber. This demonstrates that the Rayleigh wave generated by a vertical point force is insensitive to the location of the point force.

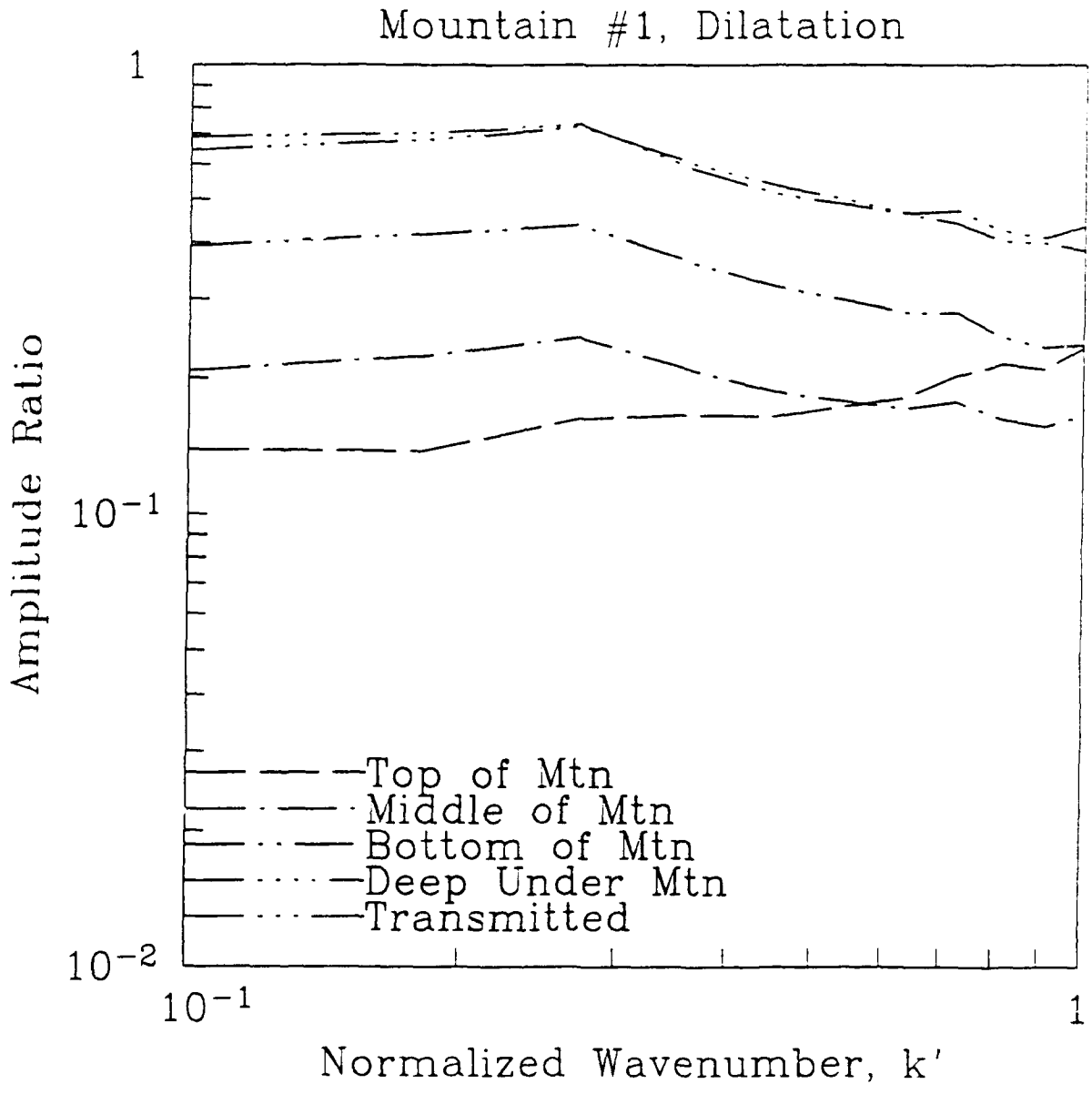

Figure 3.10. Spectral amplitude ratios for dilatational recordings at the respective source locations normalized to the incident Rayleigh wave dilatation. This demonstrates that the Rayleigh wave amplitude generated by an explosion is quite sensitive to the location of the explosion within the mountain. The Rayleigh wave amplitude is sharply reduced by location in or immediately under a mountain.

mountain, the less the effect, but a source located at the bottom of the mountain is still reduced by nearly 50% with respect to the half-space source at low frequencies.

This effect may have significant implications for long-period Rayleigh wave excitation from underground explosions placed within a mountain. The perturbation of the free surface alters the long-period response of the medium to a dilatational source much more than a vertical force. The reciprocal statement is that the free surface perturbation alters the strain field response much more than the displacement response for an incoming wavefield.

4. Moment Tensor Inversion of Five Soviet Explosions

Moment tensor inversions were performed for five explosions at the Soviet Shagan River test site. The inversions were performed using the Moment Tensor Inversion module of the Yield Estimation System (Murphy, *et al.*, 1990). The algorithms used in the inversion are equivalent to those used by Given and Mellman (1986), using surface wave path corrections derived by Stevens (1986) and Stevens and McLaughlin (1988). The inversions used data from GDSN, CDSN, and NORESS stations. Secondary station corrections were derived from a set of 20 Shagan River explosions.

The results of the moment tensor inversions are shown in the table below, and the data fits are shown in Figures 4.1 - 4.5. Data fits are excellent for all five events. The Shagan River explosion of 14 September, 1988, the Soviet JVE test, has an F factor of 0.2, a relatively low level of tectonic release compared to other Shagan River explosions.

Event	M_I (10^{14} N-m)	F	Strike (deg)
04Aug1979	157	0.33	312
28Oct1979	146	0.34	329
23Dec1979	98	0.43	315
18Oct1981	127	0.29	320
JVE	151	0.20	316

Walter and Patton (1990) analyzed the regional, broadband recordings of the JVE at the three University of Nevada Reno stations (see next section). Using 10-20 second Love waves and high-frequency SmS phases, they inferred an explosion moment of between 1.7 x 10^{16} and 2.4 x 10^{16}, with an F factor between 0.31 and 0.44. Both the explosion moment and the F factor are too high to be consistent with the long period data analyzed here. This difference could be due to the limited distribution of the U.N. Reno stations, or it could also indicate a frequency dependence in the isotropic or double-couple moments. During the next year, we plan to do a joint inversion of the regional and long period data to resolve this question.

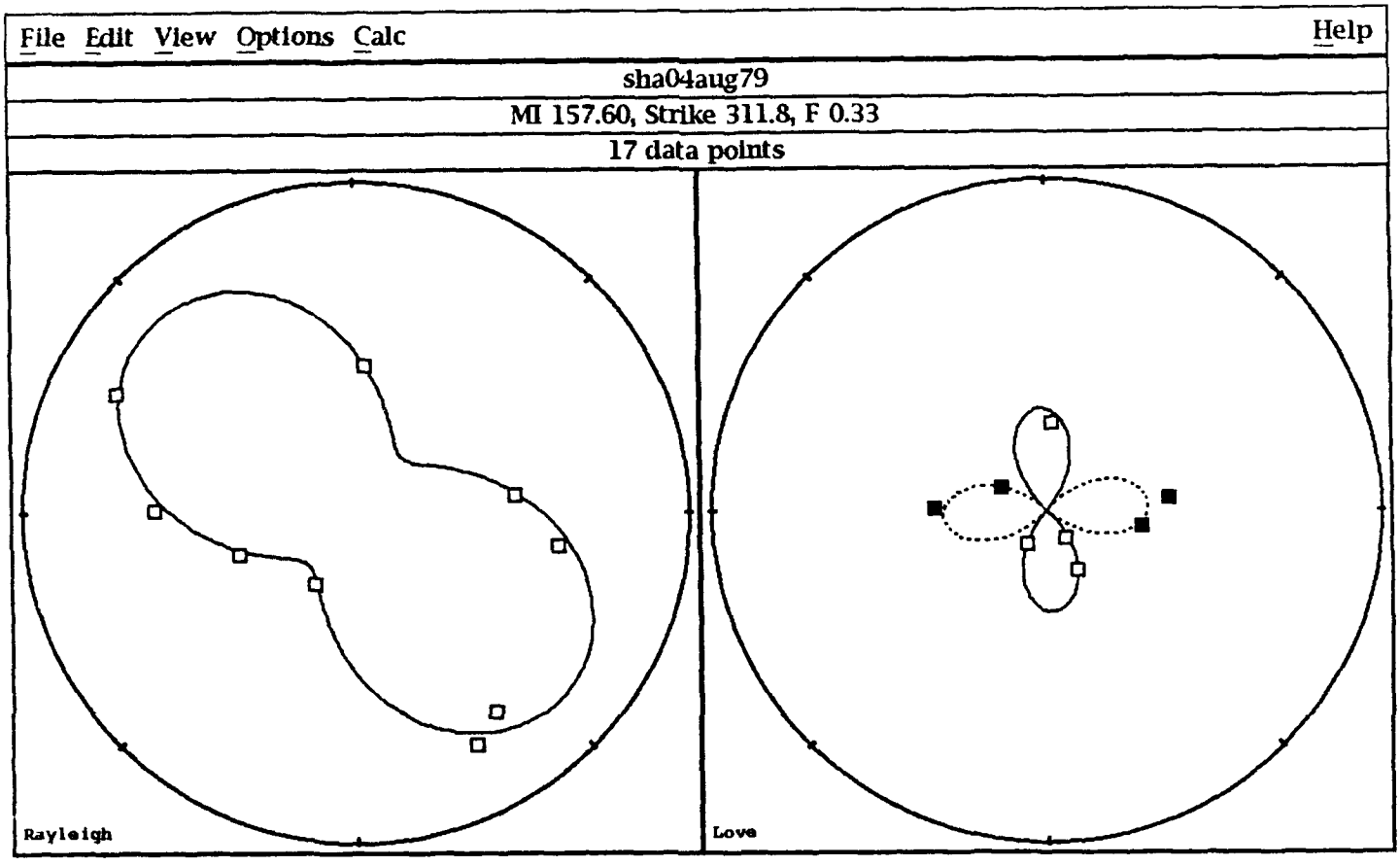

Figure 4.1. Moment tensor inversion results for the Shagan River explosion of August 4, 1979. Open squares indicate positive phase, solid squares negative. The solid line indicates positive predicted phases, dashed line negative.

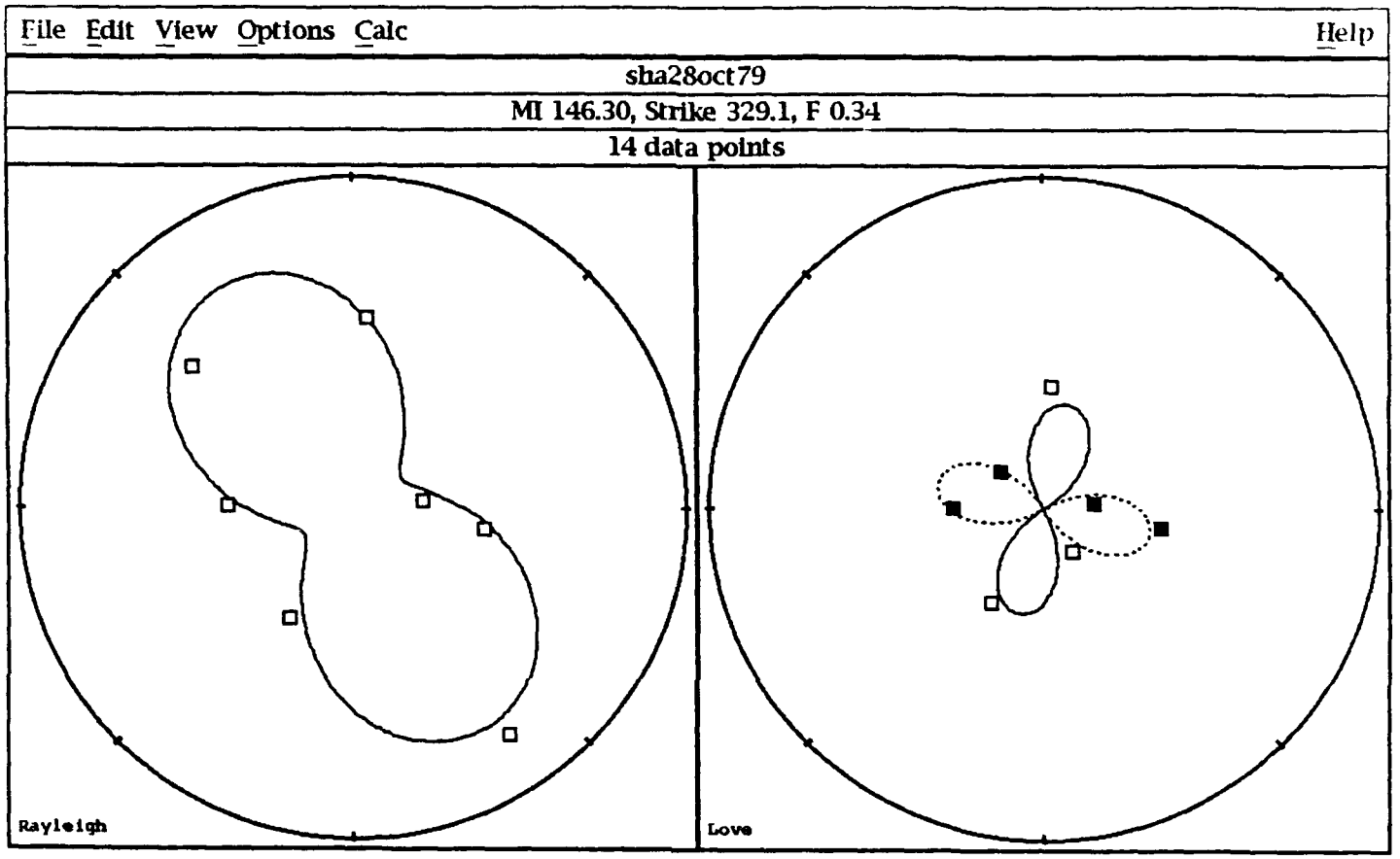

Figure 4.2. Moment tensor inversion results for the Shagan River explosion of October 28, 1979.

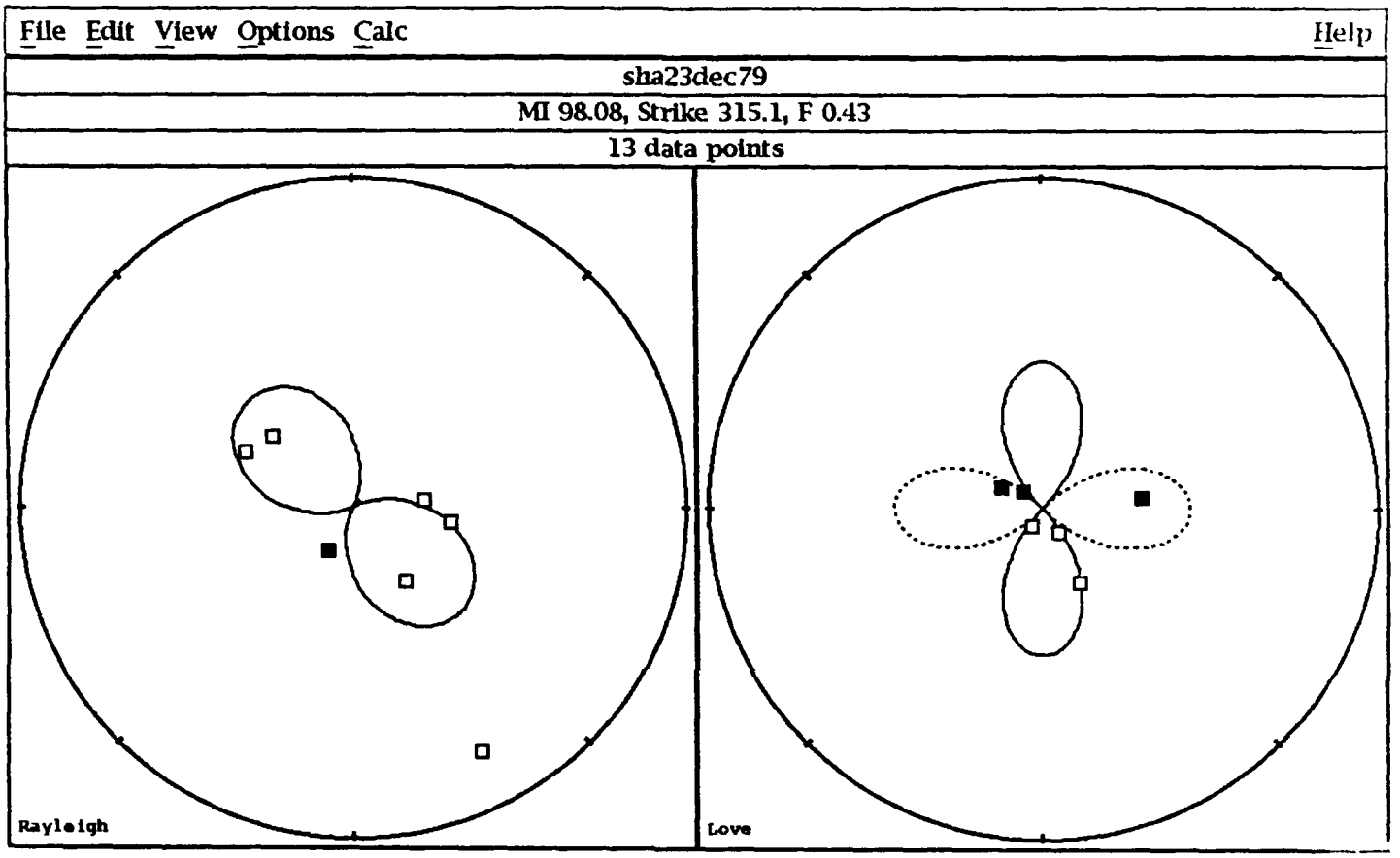

Figure 4.3. Moment tensor inversion results for the Shagan River explosion of December 23, 1979.

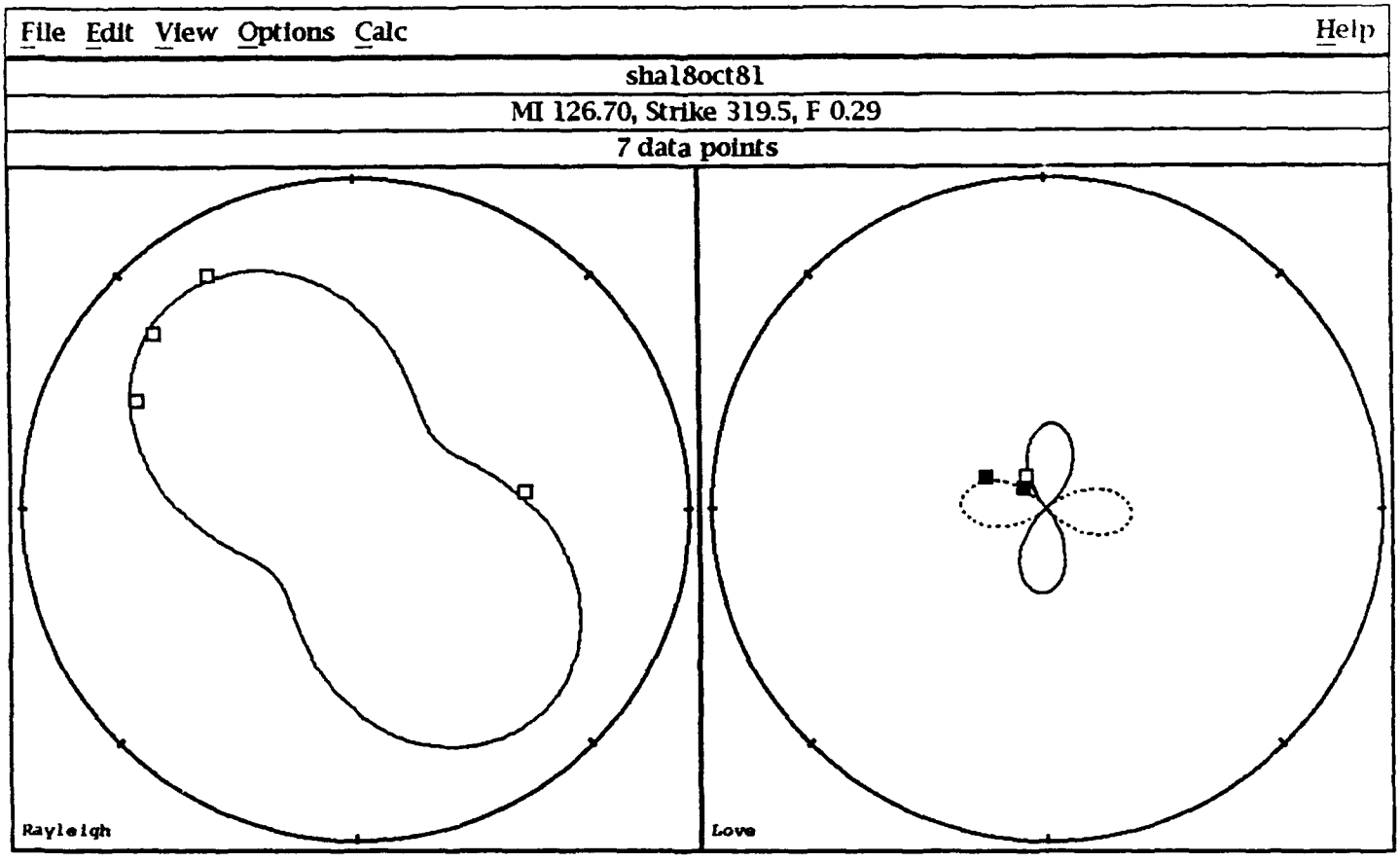

Figure 4.4. Moment tensor inversion results for the Shagan River explosion of October 18, 1981.

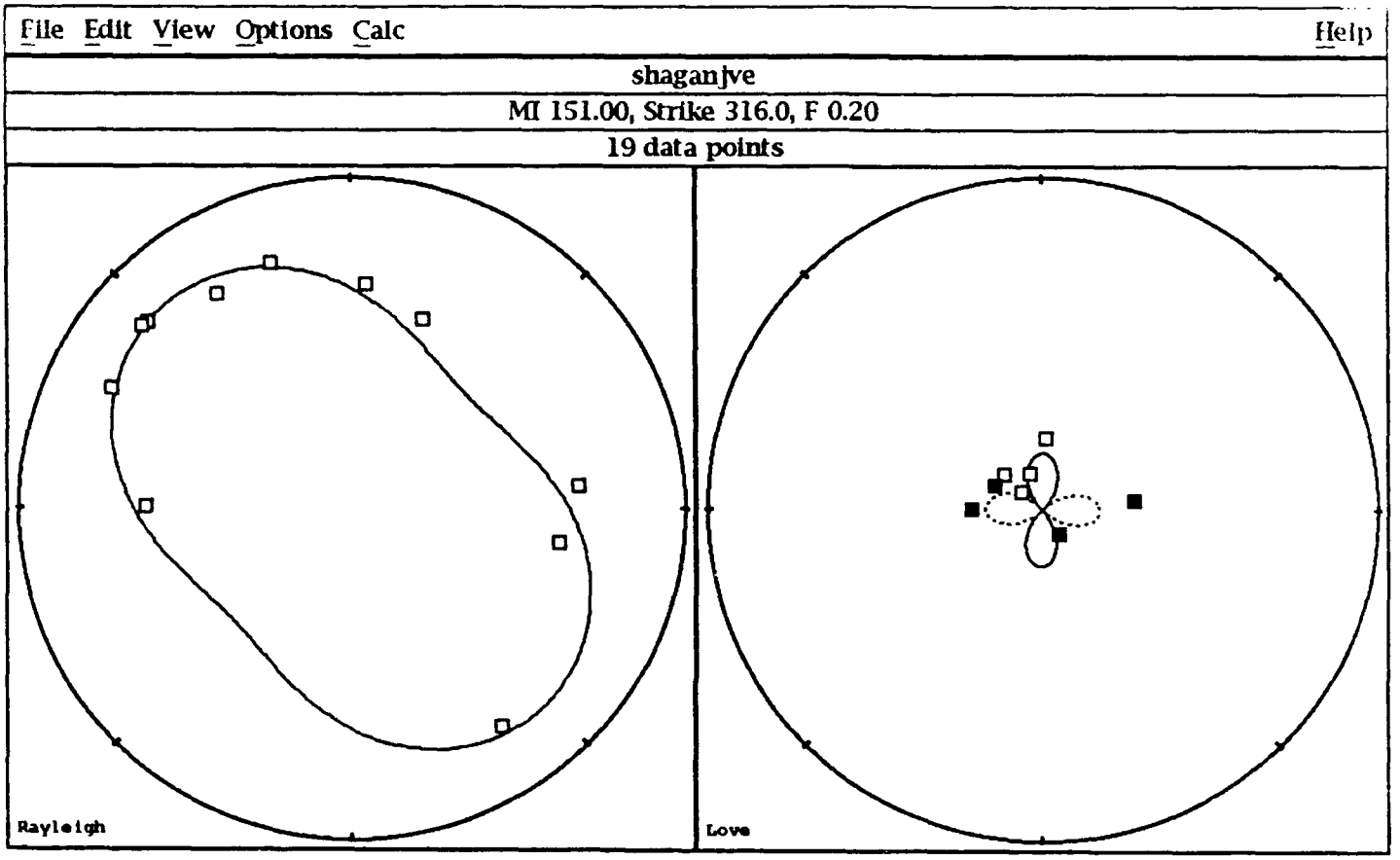

Figure 4.5. Moment tensor inversion results for the Shagan River explosion of September 14, 1988 (JVE).

5. Inversion of Regional JVE Data

Three stations operated by the University of Nevada at Reno were operating within 300 km of the Soviet JVE of September, 1988. The locations of these stations are shown in Figure 5.1. Rayleigh waves recorded at these stations were inverted to determine the shear velocity in the crust along paths from the Shagan River test site to these stations. At stations BAY and KSU, we were able to recover dispersion curves over a frequency band of 0.1 to 0.8 Hz. This allows resolution of the shear velocity structure to a depth of approximately 30 km. The surface waves at KKL showed more evidence of multipathing and it was difficult to recover consistent group velocity curves.

The results of the inversions are shown in Figure 5.2. The top figure for each station shows the inferred shear velocity for each path, and the bottom figure shows the phase and group velocities measured for each path, and predicted from the structure. Although ideally it would be better to have dispersion curves for multiple events, the data fits are quite good and the shear velocity structures should be accurate for BAY and KSU. As mentioned above, the dispersion curves at KKL are less reliable than those at the other two stations, so details of the structure, such as the low velocity zone at 15 km, may not be realistic.

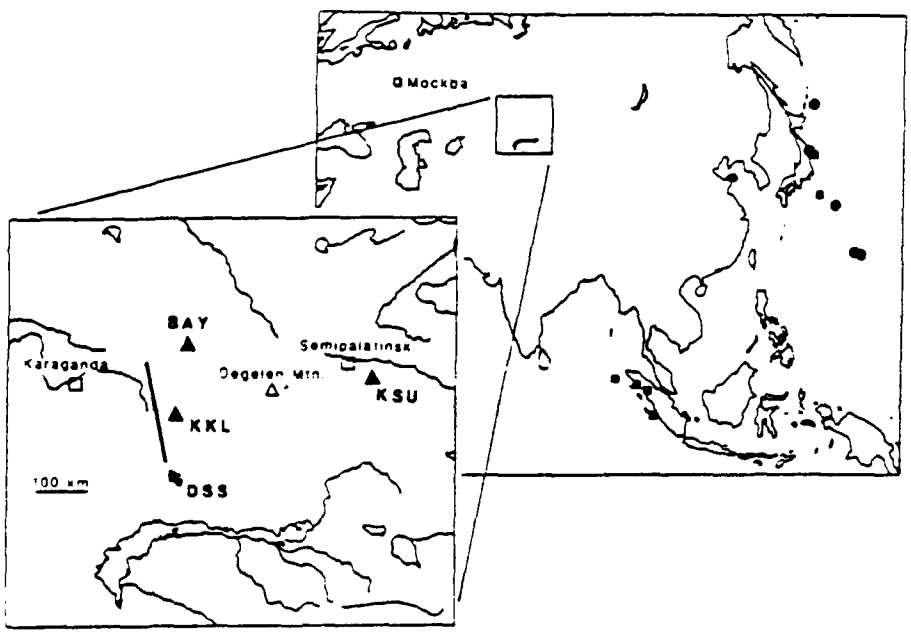

Figure 5.1. Locations of 3 stations operated by the University of Nevada at Reno that recorded the JVE (from Priestley, *et al.*, 1988).

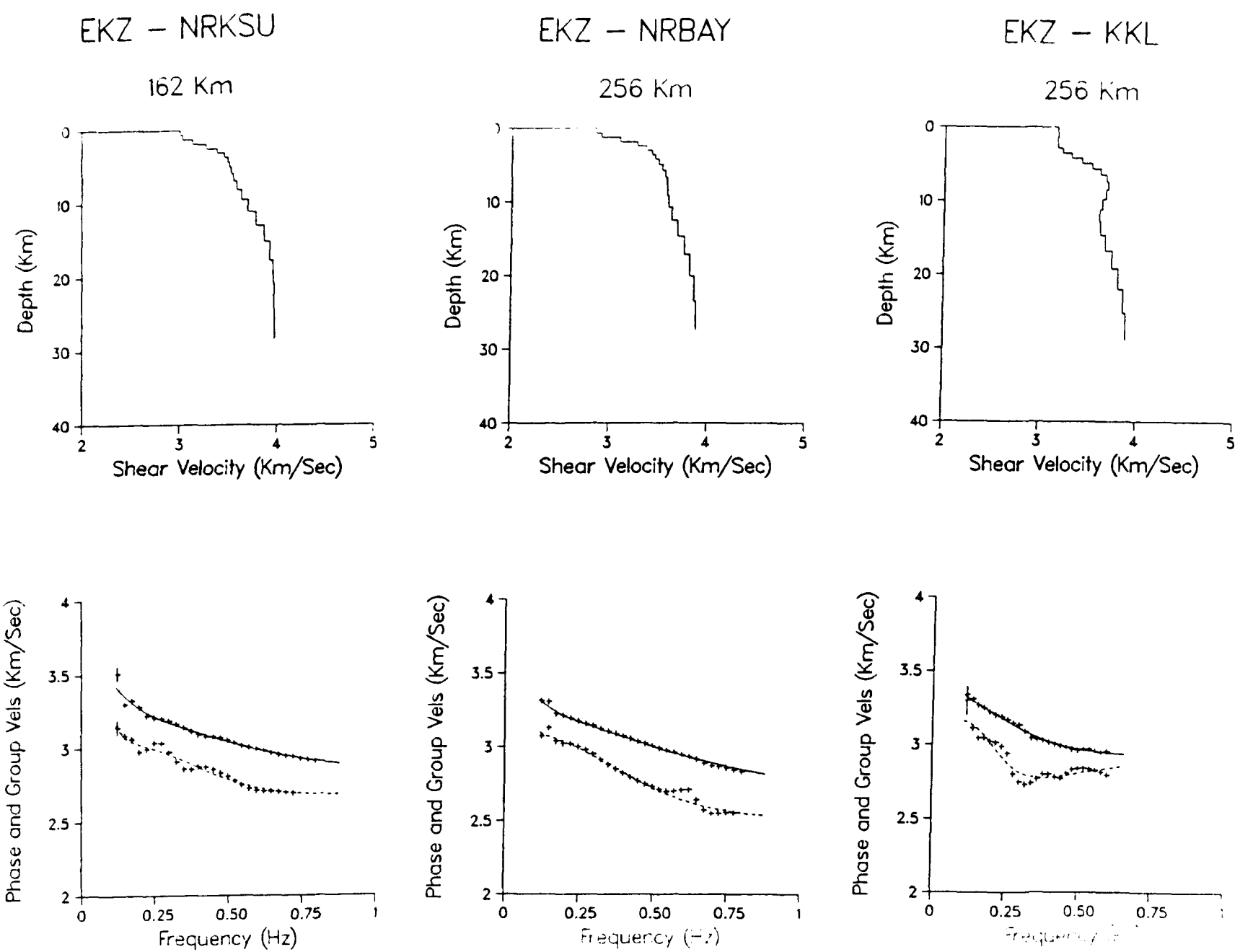

Figure 5.2. Shear velocity structures and observed and calculated phase and group velocities for paths from the Soviet JVE to KSU (left) at 162 km, BAY (middle) at 256 km and KKL (right) at 256 km.

6. Maximum Likelihood Analysis of the Bocharov Data Set.

Release of Soviet yields and yield ranges in the paper by Bocharov, *et al.* (1989) provides a unique opportunity to improve magnitude/yield estimates for Soviet test sites. The paper gives yields for 19 events and yield ranges for an additional 69 events. Maximum likelihood procedures (e.g. McLaughlin, *et al*, 1986), allow the yield ranges to be used in addition to the yield data points to reduce the uncertainties in the magnitude/yield relation. In the following analysis, UK magnitudes from Vergino (1989) were used in the maximum likelihood analysis to estimate a linear magnitude/yield relation and to estimate the mean magnitude for 20 KT.

In Figure 6.1, we show the yields and yield ranges plotted as a function of magnitude, together with a set of trial magnitude yield curves that fit the data. Notice that the yield ranges are particularly helpful in defining the magnitude yield curve near 20 kilotons which is the boundary of two yield ranges. This is shown in more detail in Figure 6.2. The large number of data points defined to be either less than or greater than 20 kilotons defines the magnitude for this yield to be 5.530 ± 0.016 (based on UK magnitudes).

The final result of the maximum likelihood analysis is the following magnitude/yield relation:

$$mb = 4.52 \pm 0.063 + 0.76 \pm 0.04 \log(W)$$

where W is the explosion yield. The standard deviation of the magnitude yield relation at 20 KT is 0.059 ± 0.012. The magnitude for a 150 KT explosion is 6.247 ± 0.047, and the standard deviation of the magnitude yield curve at 150 KT is 0.072 ± 0.019.

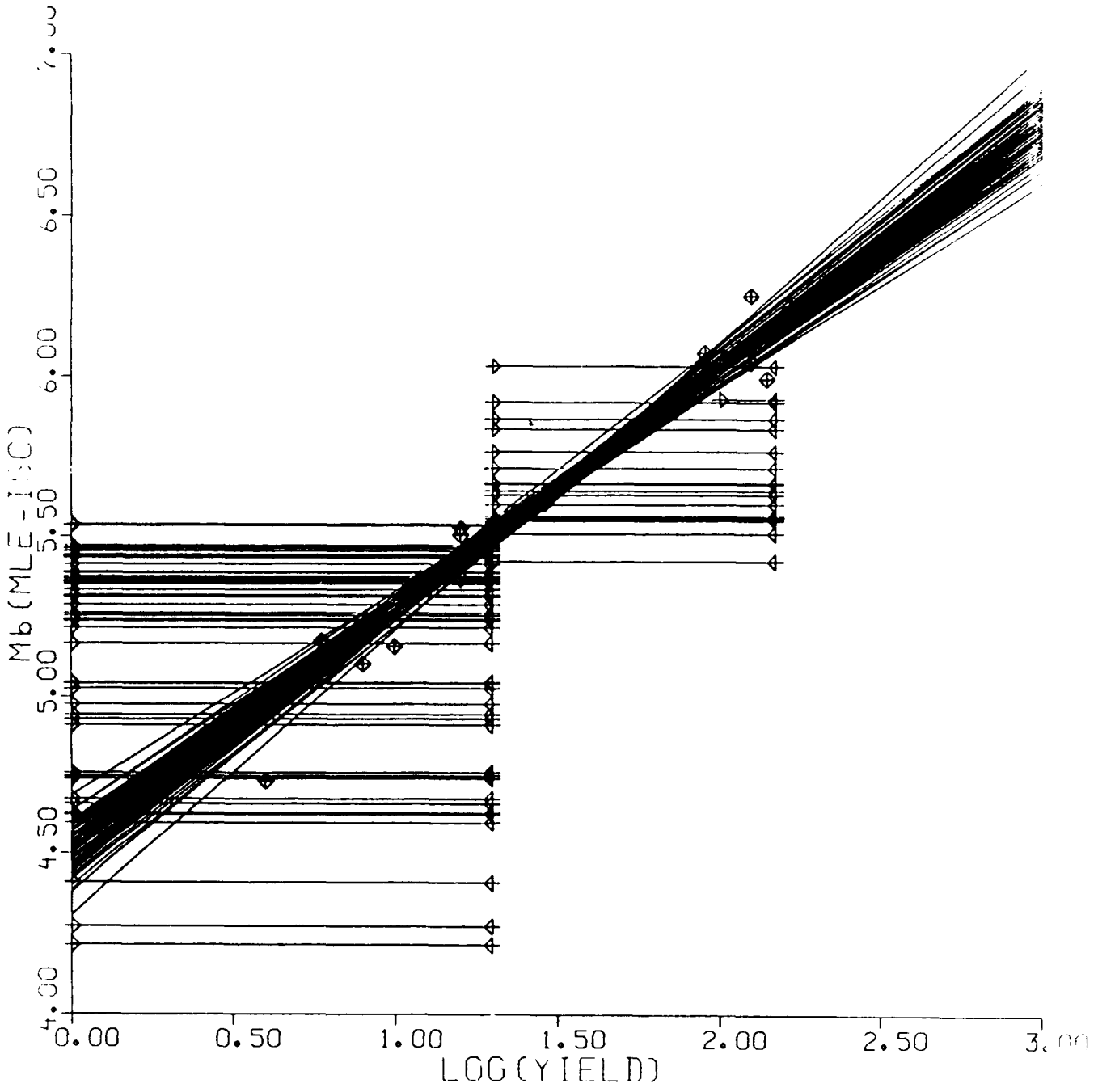

Figure 6.1. Yields and yield ranges from Bocharov, *et al.* (1989) plotted vs. UK P-wave magnitudes, together with 1 set of trial magnitude/yield relations.

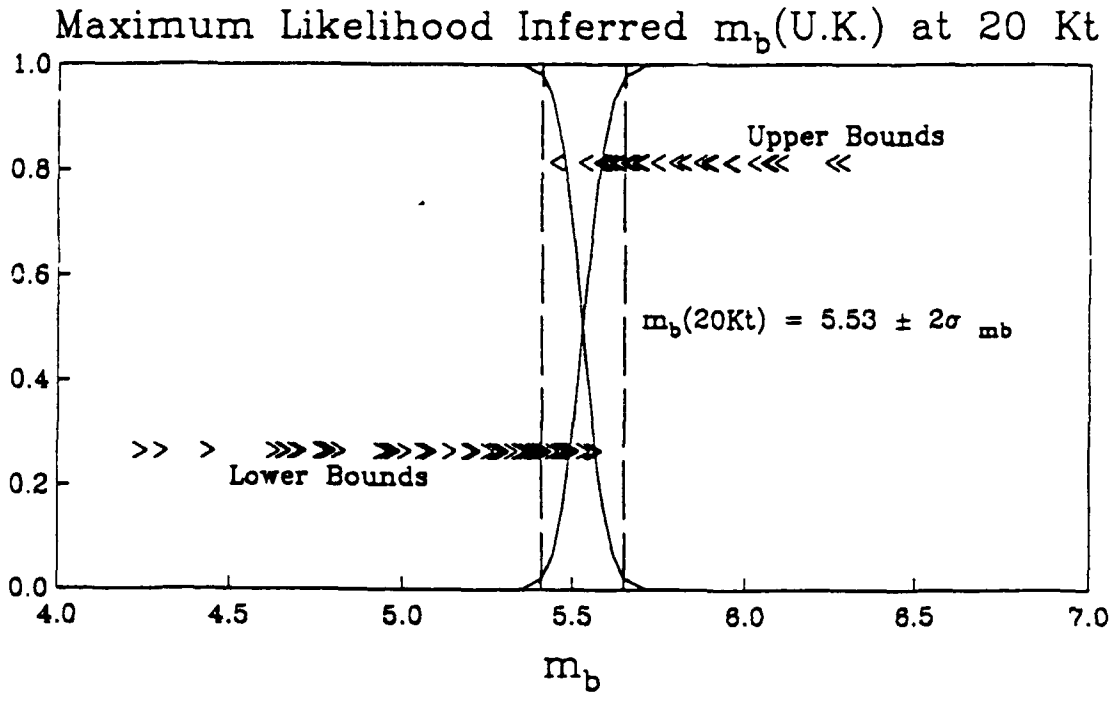

Figure 6.2. Maximum likelihood m_b at 20 KT derived from the Bocharov data set.

References

Bocharov, V. S., S. A. Zelentsov and V. N. Mikhailov (1989), "Characteristics of 96 Underground Nuclear Explosions at the Semipalatinsk Test Site," Atomic Energy (Atomnaya Energiya), *67, 3* (in Russian).

Boyd, T. M. and K. C. Creager, (1991), "The Geometry of Aleutian Subduction: Three-Dimensional Seismic Imaging," *J. Geophys. Res., 96, pp. 2267-2291,* February.

DMA (1983), "Omega, South Pacific Ocean, Isles Tuamotu (Eastern Part): HAO to FANGATAUFA," Defense Mapping Agency map number 83024.

Dziewonski, A. and D. Anderson (1983). "Travel Times and Station Corrections for P-waves at Teleseismic Distances," *J. Geophys. Res., 88,* 3295-3314.

Given, J. W. and G. R. Mellman (1986). Estimating Explosion and Tectonic Release Source Parameters of Underground Nuclear Explosions from Rayleigh and Love Wave Observations, AFGL-TR-86-0171, Sierra Geophysics, WA.

Lambert, D. G., D. H. von Seggern, S. S. Alexander, and G. A. Galt (1969). The LONG SHOT Experiment, Comprehensive Analysis, SDL Report 234, Teledyne Geotech, Alexandria, VA.

McLaughlin, K. L., T. G. Barker, S. M. Day, B. Shkoller, and J. L. Stevens (1991). Effects of Subduction Zone Structure on the Propagation of Explosion-Generated Long-Period Rayleigh Waves, S-CUBED Technical Report submitted to AFTAC, SSS-TR-91-12132.

McLaughlin, K. L., R. H. Shumway, R. O Ahner, M. E. Marshall, T. W. McElfresh, and R. A. Wagner, (1986). Determination of Event Magnitudes with Correlated Data and Censoring: a Maximum Likelihood Approach, TGAL-TR-86-01.

Murphy, J. R. (1990), "A New System for Seismic Yield Estimation of Underground Explosions," *12th Annual DARPA/GL Seismic Research Symposium, September 18-20, Key West, FL, Proceedings, 384-390.*

Olsen, K. H., J. N. Stewart, J. E. McNeil, and M. J. Vitousek (1972), "Long-Period Water-Wave Measurements for the Milrow and Cannikin Nuclear Explosions," *Bull. Seism. Soc. Am., V. 62.,* 1559-1578.

Priestly, K. F., G. Zandt, and G. Randall (1988), "Crustal Structure in Eastern Kazakh, U.S.S.R. from Teleseismic Receiver Functions," *Geophysical Research Letters, V. 15,* 613-616.

Stevens, J. L. (1986a). "Estimation of Scalar Moments from Explosion-Generated Surface Waves," *Bull. Seism. Soc. Am., 76,* 123-151.

Stevens, J. L. (1986b). Analysis of Explosion-Generated Rayleigh and Love Waves from East Kazakh, Amchitka, and Nevada Test Sites. AFGL-TR-86-0043.

Stevens, J. L. and K. L. McLaughlin (1988), Analysis of Surface Waves from the Novaya Zemlya, Mururoa, and Amchitka Test Sites, and Maximum Likelihood Estimation of Scalar Moments from Earthquakes and Explosions, Technical Report submitted to Air Force Technical Application Center, SSS-TR-89-9953.

Stevens, J. L., S. M. Day, K. L. McLaughlin and B. Shkoller (1991). Two-Dimensional Axisymmetric Calculations of Surface Waves Generated by an Explosion on an Island, S-CUBED Technical Report submitted to AFTAC, SSS-TR-91-12133.

Toksoz, M. N. and H. H. Kehrer (1972). "Tectonic Strain Release Characteristics of CANNIKIN," *Bull Seism. Soc. Am., 62,* 1425-1438.

von Seggern, D. (1978), Intersite Magnitude-Yield Bias Exemplified by the Underground Nuclear Explosions MILROW, BOXCAR, and HANDLEY, Teledyne Geotech Report SDAC-TR-77-4.

Vergino E. (1989), "Soviet Test Yields," *EOS, V. 70, No. 48,* 1511-1525, November 28.

Walter, W. R. and H. Patton (1990), "Tectonic Release from the Soviet Joint Verification Experiment," *Geophysical Research Letters, V. 17, No. 10,* 1517-1520.

DISTRIBUTION LIST
FOR UNCLASSIFIED REPORTS
DARPA-FUNDED PROJECTS
(Last Revised: 26 Sep 89)

RECIPIENT	NUMBER OF COPIES
DEPARTMENT OF DEFENSE	
DARPA/NMRO ATTN: Dr. R. Alewine and Dr. A. Ryall 1400 Wilson Boulevard Arlington, VA 22209-2308	2
Defense Intelligence Agency Directorate for Scientific and Technical Intelligence Washington, D.C. 20340-6158	1
Defense Nuclear Agency Shock Physics Directorate/SD Washington, D.C. 20305-1000	1
Defense Technical Information Center Cameron Station Alexandria, VA 22314	2
DEPARTMENT OF THE AIR FORCE	
AFOSR/NP Bldg 410, Room C222 Bolling AFB, Washington, D.C. 20332-6448	1
AFTAC/STINFO Patrick AFB, FL 32925-6001	1
AFTAC/TT Patrick AFB, FL 32925-6001	3
AFWL/NTESG Kirkland AFB, NM 87171-6008	1
GL/LWH ATTN: Mr. James Lewkowicz Terrestrial Sciences Division Hanscom AFB, MA 01731-5000	1

DEPARTMENT OF THE NAVY

NORDA 1
ATTN: Dr. J. A. Ballard
Code 543
NSTL Station, MS 39529

DEPARTMENT OF ENERGY

Department of Energy 1
ATTN: Mr. Max A. Koontz (DP-331)
International Security Affairs
1000 Independence Avenue
Washington, D.C. 20585

Lawrence Livermore National Laboratory 3
ATTN: Dr. J. Hannon, Dr. S. Taylor, and Dr. K. Nakanishi
University of California
P.O. Box 808
Livermore, CA 94550

Los Alamos Scientific Laboratory 2
ATTN: Dr. C. Newton
P.O. Box 1663
Los Alamos, NM 87544

Sandia National Laboratories 1
ATTN: Mr. P. Stokes, Dept. 9110
P.O. Box 5800
Albuquerque, NM 87185

OTHER GOVERNMENT AGENCIES

Central Intelligence Agency 1
ATTN: Dr. L. Turnbull
OSI/NED, Room 5G48
Washington, D.C. 20505

U. S. Arms Control and Disarmament Agency 1
ATTN: Dr. M. Eimer
Verification and Intelligence Bureau, Rm 4953
Washington, D.C. 20451

U. S. Arms Control and Disarmament Agency 1
ATTN: Mr. R. J. Morrow
Multilateral Affairs Bureau, Rm 5499
Washington, D.C. 20451

U. S. Geological Survey 1
ATTN: Dr. T. Hanks
National Earthquake Research Center
345 Middlefield Road
Menlo Park, CA 94025

OTHER GOVERNMENT AGENCIES (continued)

U. S. Geological Survey MS-913 1
ATTN: Dr. R. Masse
Global Seismology Branch
Box 25046, Stop 967
Denver Federal Center
Denver, CO 80225

UNIVERSITIES

California Institute of Technology 1
ATTN: Dr. D. Harkrider
Seismological Laboratory
Pasadena, CA 91125

Columbia University 1
ATTN: Dr. L. Sykes
Lamont-Doherty Geological Observatory
Palisades, NY 10964

Cornell University 1
ATTN: Dr. M. Barazangi
INSTOC
Snee Hall
Ithaca, NY I4853

Harvard University 1
ATTN: Dr. J. Woodhouse
Hoffman Laboratory
20 Oxford Street
Cambridge, MA 02138

Massachusetts Institute of Technology 1
ATTN: Dr. T. Jordan
Department of Earth and Planetary Sciences
Cambridge, MA 02139

Southern Methodist University 2
ATTN: Dr. E. Herrin and Dr. B. Stump
Geophysical Laboratory
Dallas, TX 75275

DEPARTMENT OF DEFENSE CONTRACTORS

Center for Seismic Studies 2
ATTN: Dr. C. Romney and Mr. R. Perez
1300 N. 17th Street, Suite 1450
Arlington, VA 22209

ENSCO, Inc. 1
ATTN: Dr. R. Kemerait
445 Pineda Court
Melbourne, FL 32940-7508

Pacific Sierra Research Corp. 1
ATTN: Mr. F. Thomas
12340 Santa Monica Boulevard
Los Angeles, CA 90025

Science Applications International Corporation 1
ATTN: Document Control (Dr. T. Bache, Jr.)
10260 Campus Point Drive
San Diego, CA 92121

Science Horizons 2
ATTN: Dr. T. Cherry and Dr. J. Minster
710 Encinitas Blvd.
Suite 101
Encinitas, CA 92024

S-CUBED, A Division of Maxwell 1
Laboratories, Inc.
ATTN: Dr Jeff Stevens
P.O. Box 1620
La Jolla, CA 92038-1620

Sierra Geophysics, Inc. 2
ATTN: Dr. R. Hart and Dr. G. Mellman
11255 Kirkland Way
Kirkland, WA 98033

OTHER DISTRIBUTION

To be determined by the project office 7

TOTAL 50